We would like to sincerely thank the reviewer for his comments. We believe they help us to improve the manuscript significantly and give us many useful suggestions to improve the mission. We have corrected the manuscript according reviewer's comments and answer the reviewer's question point by point below.

Reviewer comments are in italic blue, the manuscript modifications are in red. The answer "Done" means that the manuscript has been modified following exactly the reviewer comment.

Reply to general comments

1) Where the two instruments differ is in the spectrometers used. EOS MLS has oldfashioned filter banks, whereas TALIS will use FFT spectrometers with many more channels. For this paper to demonstrate any novelty, it needs to show how the coverage of the TALIS spectrometers differs from that of the MLS filter banks, and to demonstrate the extent to which the improved coverage leads to improved quality of retrieval products. This would involve simulating retrievals with the two sorts of spectrometers, with all other factors kept identical.

Reply: We agree that spectrometer is the major difference between the two instruments. Figure 3 has been added to show the coverage of the TALIS spectrometers differs from that of the MLS filter banks. (see specific comments)

Section 4.2 is added to show the performance comparison between TALIS FFT spectrometer and MLS 'Standard' 25-channel spectrometer (Fig.9 to 11):

"As discussed in section 2.2, TALIS has similar bands to EOS MLS. The major difference between these two instruments is the spectrometers used in limb sounding. A simulation is performed to compare the performance of the main products between TALIS FFT spectrometer and EOS MLS 'Standard' 25-channel spectrometer. Figure 9 to 11 show the retrieval products of TALIS and MLS, all the factors are identical except the spectrometer.

According to the simulation results, TALIS can do a better job than EOS MLS because of the wider bandwidth and finer resolution. Temperature precision of TALIS is improved 1–2 K compared with EOS MLS and the vertical resolution is improved about 2 km. H_2O precision is improved about 2–10 %. O_3 precision is improved about 2–20 % and retrieved well in the mesosphere".

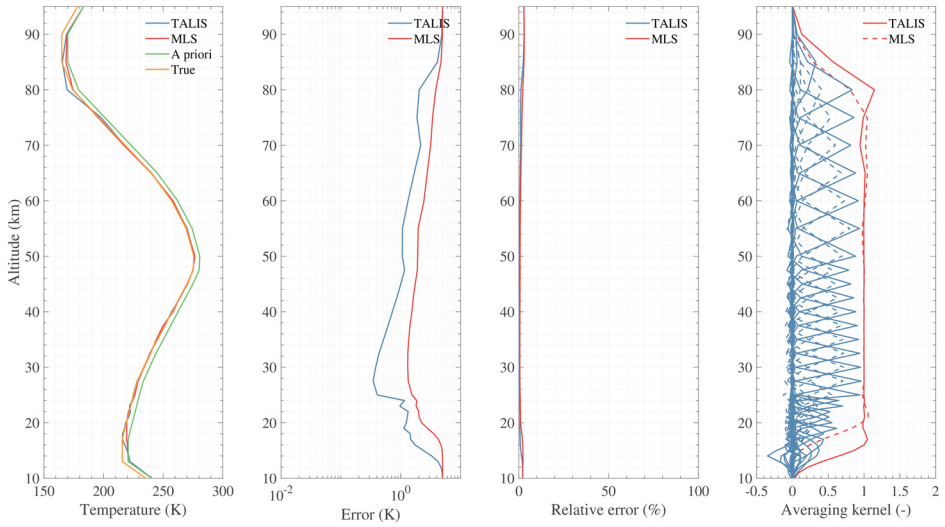

Figure 9. Temperature product comparison between TALIS FFT spectrometer and MLS 'Standard' spectrometer using 118.75 GHz line. All other factors are identical.

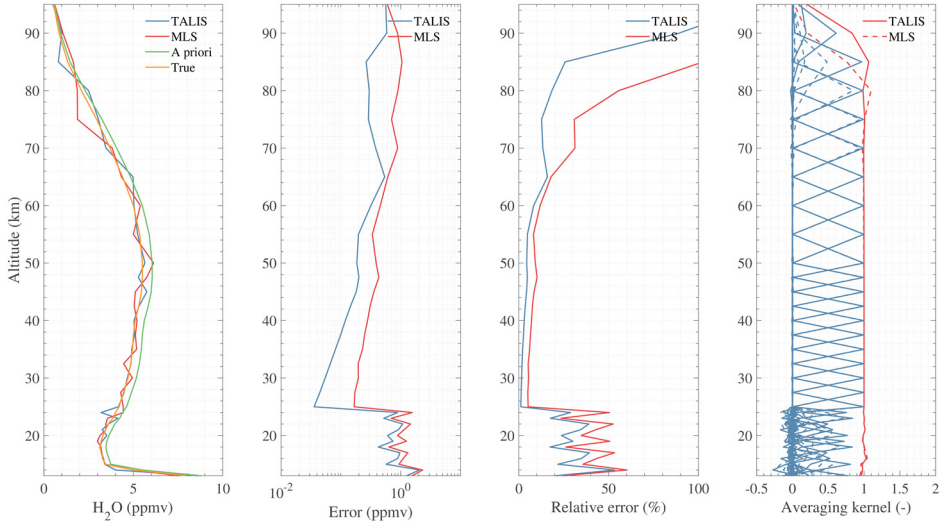

Figure 10. H_2O product comparison between TALIS FFT spectrometer and MLS 'Standard' spectrometer using 183.31 GHz line. All other factors are identical.

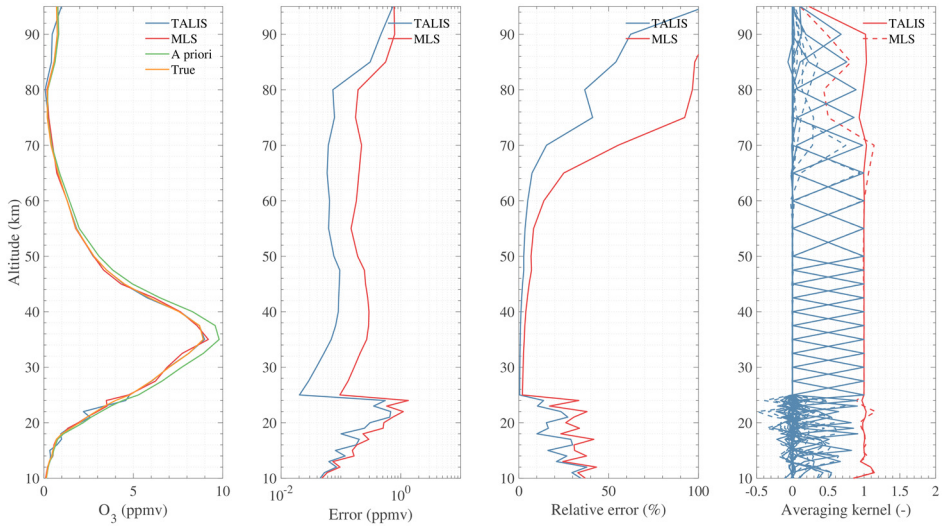

Figure 11. O_3 product comparison between TALIS FFT spectrometer and MLS 'Standard' spectrometer using 235.71 GHz line. All other factors are identical.

2) The simulation reported has a number of failings. The most serious of these are the failure to properly consider the vertical resolution of the instrument, and the failure to describe the antenna characteristics assumed; these characteristics are the main factor limiting the vertical resolution of the instrument. For the paper to be published, the antenna characteristics should be described, and the inevitable tradeoff between resolution and precision considered properly. Another problem is the failure to address how information on the geometrical tangent height is to be incorporated into the retrieval of temperature and tangent pressure.

Reply: We are sorry to omit these characteristics. Section 2.1 has been rephrased, more details about TALIS are added:

"The TALIS payload (Fig. 1) and its proposed scan characteristics are summarized in Table 1. The instrument will be set at a sun-synchronous orbit at a normal altitude of 600 km. The offset parabolic antenna is made of a single reflector with 1.6 m projective aperture and four independent feeds. The layout of four discrete feeds is shown in Fig. 2. Compared with the quasi-optical separation layout (such as MLS), this strategy is easier and has higher observation precision. But it will lead to an observed difference of about 20 km between the four radiometers. The widths of the field of view (FOV) at the tangent point are about 5.5, 3.8, 3.3, and 0.96 km respectively. The two-point calibration method is adopted by TALIS, and an extra calibration target is set at the bottom of the antenna. The extra target can be used to improve the calibration precision and evaluate the antenna effect and nonlinearity. At the beginning of the scan, TALIS will view the hot target (ambient temperature) and the extra target (lower temperature) in 3 s, and then it will scan the limb from 0 to 100 km vertically and obtain the spectra every 1 km with an integration time of 0.1 s, finally, it views the cold space at 200 km in 5 s. The process of retrace is the same (also record data) and giving a total period of about 36 s".

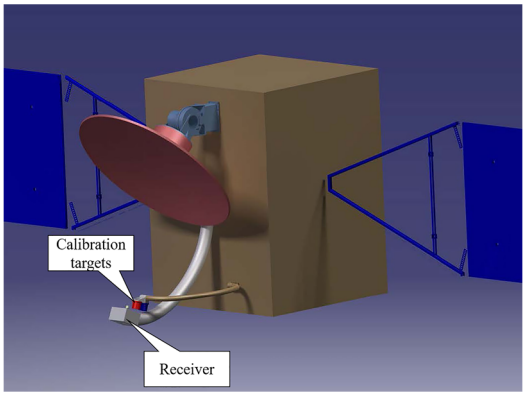

Figure 1. The schematic diagram of TALIS payload

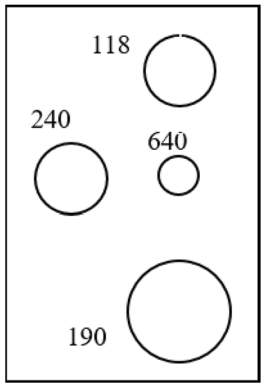

Figure 2. The layout of the four antenna feeds

Table 1. Characteristics of the TALIS payload

Satellite altitude	600 km
Scan altitude	0–100 km
LOS nadir angle	66.07–68.17° （2.1° ）
Scan velocity	0.21° s^{-1} (36 s $scan^{-1}$)
Spectrum integration time	0.1 s (1 km)
Antenna size	1.6 m
Antenna vertical FOV	5.5, 3.8, 3.3, 0.96 km
Spectrometer Bandwidth	2 GHz
Spectrometer resolution	2 MHz
LO frequency	120, 190.1, 239.66, 642.87 GHz

The proposed FOV of TALIS are 5.5, 3.8, 3.3, 0.96 km, and TALIS record the spectra every 1 km. According to the MLS study, there is a trade-off between the vertical resolution and information gained, and little information is lost by going from twelve to six surfaces per decade. Thus, we use 2.5 km in our simulation for simplicity since the FOV of TALIS are similar to MLS. We will discuss the best vertical resolution of TALIS in the future works.

The sentence in section 4.1 has been rephrased as follows (P10, L21):

"In this simulation, the scan altitude range is from 10 to 95 km and the spectra are obtained every 2.5 km. As the effective FOV of TALIS are similar to MLS, we use 2.5 km as the vertical resolution. It is the trade-off between the step of efficient limb observation and the optimum information can be obtained (Livesey and Snyder, 2004)".

The pressure and geometric height are linked by the hydrostatic equilibrium equation. The hydrostatic equilibrium equation needs the correct geometric height information of tangent point. The geometric height information is obtained by the satellite

navigation system and the antenna view angle. It is usually different between the tangent point altitude as determined by geometry and reported by the instrument, so it should be retrieved as a state vector at first.

A statement has been added to temperature retrieval as follows (P11, L19):

"Once the temperature profile is retrieved, the pressure profile can be calculated from the hydrostatic equilibrium equation using a known pressure and temperature at a reference tangent point. The pressure profile is not a direct product and is not shown here".

Reply to specific comments

Page 1 line 18: In "high single scan retrieval precision of 1 – 50%", remove the word "high". 1% can be considered high precision in this context, but 50% is not high precision in any context. I suppose you could replace "high" with "relatively high".

Reply: Done. The sentence has been rephrased as follows:

"Chemical species such as H_2O, O_3, HCl show relatively high single scan retrieval precision of 1–20% over most of the useful range and ClO, N_2O, HNO_3 can be retrieved with a precision < 50%".

Page 1 line 25–27: It seems odd to talk of this instrument as a "Terahertz limb sounder" when its highest frequency is 0.6 THz and its lowest frequency is below 0.2 THz.

Reply: Yes, it is not very appropriate but it is named by our research project.

Page 3 lines 5–7: The double sideband nature of both UARS MLS and Aura MLS has been a considerable nuisance to the instrument team, especially when attempting to obtain results in the important 300 hPa – 60 hPa range. It was a technological limitation at the time EOS MLS was built, which would have been too expensive to work around. Modern mm-wave technology includes sideband separating receivers. As TALIS appears still to be in the design phase, the authors might like to consider whether this technology would be appropriate.

Reply: We thank the reviewer for this suggestion. Sideband separating receiver has been considered and we believe it is very useful in limb sounding. However, TALIS is limited to the technology and fund, it is difficult to use this receiver. Sideband separating receiver may be adopted in the future mission.

Page 3 line 14: "TALIS covers most spectral bands of EOS MLS and extends them." It would perhaps be worth adding some sort of diagram with the EOS MLS and TALIS spectral bands overlaid on each other, so that the reader can quickly see by

how much the TALIS coverage extends that of EOS MLS. The should also be a statement that EOS MLS had a band at 2.4 THz which TALIS will lack — there is no need of a diagram to show this.

Reply: Figure 3 has been added to show the difference between MLS and TALIS spectral bands.

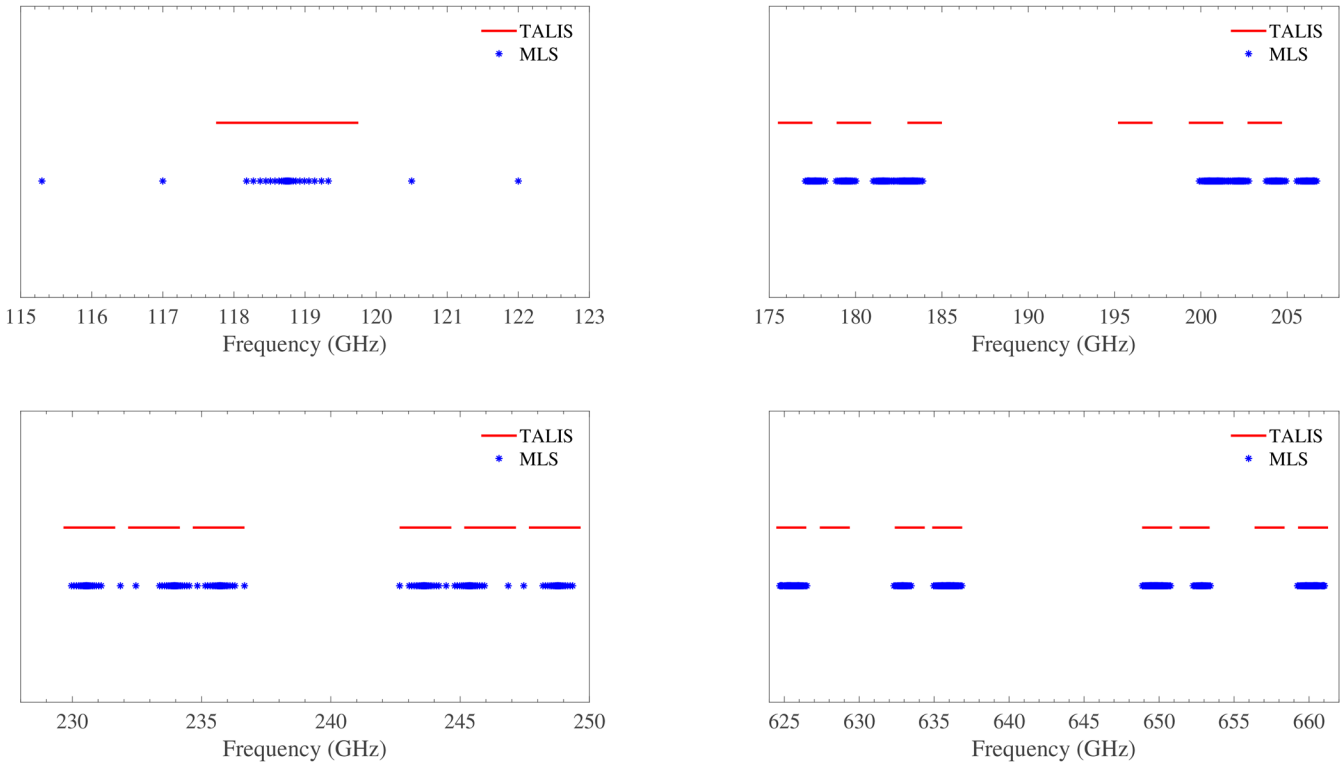

Figure 3. Spectral bands of EOS MLS and TALIS

The sentence has been rephrased as follows:

"TALIS covers most spectral bands of EOS MLS and extends them (see Fig 3), but lack the 2.4 THz band".

Page 3 line 15: "... and lower noise of TALIS". The authors should probably state the Tsys values of the EOS MLS bands so that the reader can easily see how much lower the noise level of TALIS will be. A cross-check against Waters et al. (2006) (see Table 1) indicates that the TALIS Tsys values are either effectively the same as those of EOS MLS or are about 30%–50% better. This is unlikely to be sufficient to allow easy measurement of a species which EOS MLS can not measure. If TALIS can really do a better job than EOS MLS, it is likely to be on account of the bandwidth and resolution of the spectrometers rather than because of the slightly better measurement noise.

Reply: We changed the Table 2 so that the Tsys value of TALIS and EOS MLS can be distinguished. The "lower noise" in this sentence has been removed.

The performance comparison between TALIS FFT spectrometer and MLS 'Standard' 25-channel spectrometer shows that TALIS can do a better job than EOS MLS because of the wider bandwidth and finer resolution.

Page 4 Line 10: It is worth pointing out that the only SO_2 which is observable by instruments like EOS MLS and TALIS comes from volcanic eruptions.

Reply: The sentence has been rephrased as follows:
"There is no obvious SO_2 emission with the standard profile present in the passband of 240 GHz radiometer. The only SO_2 which is observable by MLS comes from volcanic eruptions".

Page 4 Lines 12–13: ". . .MLS demonstrated that SO_2 can be measured by 240 GHz radiometer cooperated with 190 GHz radiometer . . . ". What I actually said in Pumphrey et al. (2015) is that MLS measures SO_2 from three radiometers: 190 GHz, 240GHz and 640 GHz. The radiometers are not combined with each other. Rather, a separate SO_2 product is produced from each radiometer. Only the 240 GHz SO_2 product is recommended for general use.

Reply: The sentence has been rephrased as follows:
"MLS demonstrated that SO_2 can be measured by 190 GHz, 240GHz, and 640 GHz radiometer, but only 240 GHz SO_2 product is recommended for general use".

Page 4 line 14: "NO_2 is a unique species not covered by EOS MLS". This is entirely true. The authors should perhaps explain whether TALIS's ability to measure this species is due to improved bandwidth, resolution or radiometer noise. Figure 3 suggests that the measurement will be very difficult.

Reply: TALIS's bandwidth and resolution are enough to detect the NO_2. However, the intensity of NO_2 emission is very weak, as the simulation result (Fig. 19) shows that only averaged measurements can be used to retrieve NO_2 profile.

The sentence has been rephrased as follows:
"NO_2 is a unique species not covered by EOS MLS, and TALIS's wider bandwidth and finer resolution have the potential ability to measure it".

Page 8 line 5: This formula defines the Planck brightness temperature. It is not uncommon in microwave remote sensing (especially in limb sounding) to work with the Rayleigh-Jeans brightness temperature because it is proportional to the radiance. The authors should be clear which brightness temperature they intend to use.

Reply: We agree that it is common to work with the Rayleigh-Jeans brightness temperature in limb sounding. However, Planck's radiation law is the standard formula transform radiance to blackbody's absolute temperature. Rayleigh-Jeans law is the approximation to Planck's law and its linear transformation will make the calculation simpler. But as the reference said, Rayleigh-Jeans law will lead to a brightness temperature error which varies with frequency and temperature. Thus, we want to use Planck function since it is widely used in the meteorological satellites all over the world such as Advanced Microwave Technology Sounder (ATMS) and FY-3 Microwave Humidity and Temperature Sounder (MWHTS). We will study the impact of these two different formulas in the future works.

Reference:

Weng, Fuzhong and Zou, Xiaolei.: Errors from Rayleigh–Jeans approximation in satellite microwave radiometer calibration systems, Applied Optics, 52, 505–508, https://doi.org/10.1364/AO.52.000505, 2013

We added a statement at the last of section 3.1 as follows:

"The measured radiance is transformed to brightness temperatures using the Planck's function".

Page 10 section 4.1: This section omits a number of important items. Firstly, it does not state what antenna pattern is assumed when applying equation (5). This is important because the antenna pattern is the main limitation on vertical resolution. The pattern does not always vary with frequency in the way one would naively expect. The 640GHz band of EOS MLS has better vertical resolution than the 190 GHz band, but nowhere near the three times better that you would expect from Rayleigh's criterion. This is because the 640GHz radiometer does not view the full aperture of the antenna. Secondly, nothing is said about the specific problem of temperature/pressure retrieval. We usually have two sources of information about where the antenna is pointing: pressure information that comes from the radiance measurements, and geometric height information which comes from the satellite navigation system and the antenna view angle. These two pieces of information are linked by the hydrostatic equation, which itself depends on the temperature profile. For the temperature retrieval precisions presented to be credible, the reader needs to know how the geometric tangent height information was incorporated, and how precise it was assumed to be.

Reply: We are sorry to omit these items and they are now added. The simulation antenna patterns have been added in Figure 8. The instrument field of view (FOV) are about 5.5, 3.8, 3.3, and 0.96 km respectively. Actually, we don't consider the antenna pattern in performance simulation because of the large computation time.

A statement has been added as follows:

"The simulation antenna patterns of the four radiometers are shown in Fig. 8. As the antenna calibration can be done by a linear function, it has no impact on the following simulation, so antenna pattern is not added in simulation below".

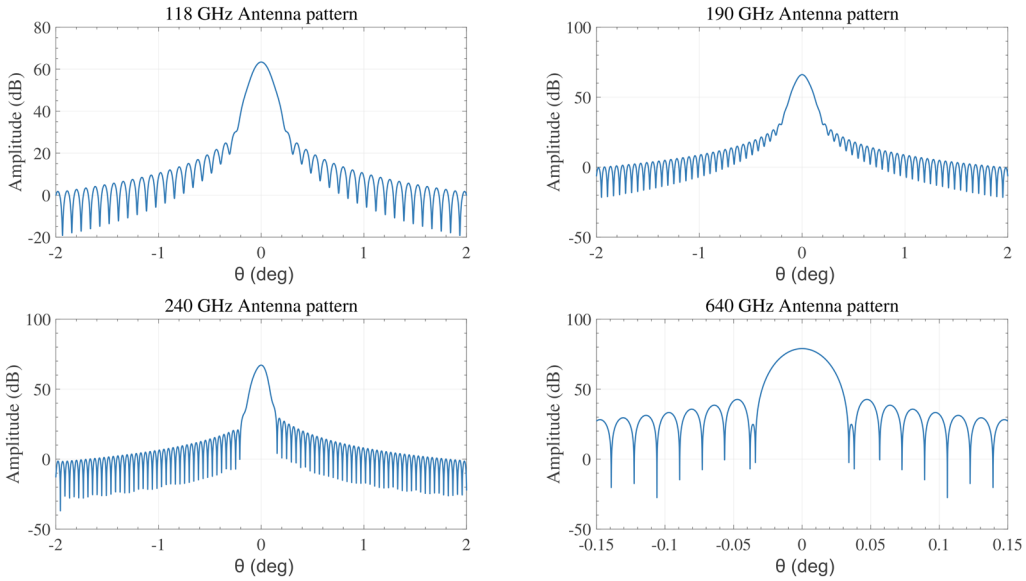

Figure 8. The antenna patterns of TALIS

The pressure and geometric height are linked by the hydrostatic equilibrium equation. The hydrostatic equilibrium equation needs the correct geometric height information of tangent point. The geometric height information is obtained by the satellite navigation system and the antenna view angle. It is usually different between the tangent point altitude as determined by geometry and reported by the instrument, so it should be retrieved as a state vector at first.

A statement has been added to temperature retrieval as follows (P11, L19):

"Once the temperature profile is retrieved, the pressure profile can be calculated from the hydrostatic equilibrium equation using a known pressure and temperature at a reference tangent point. The pressure profile is not a direct product and is not shown here".

Page 14, figures 6–10: The precision becomes very much poorer very suddenly at a height of 25 km. The authors should explain why this is. The figures make it appear as if the retrieval grid changes vertical resolution at this point from a grid which is coarser than the achievable vertical resolution to one which is finer than the achievable vertical resolution. This will inevitably make the retrieval precision appear far worse below 25 km, but this does not mean that the performance of the instrument itself is far worse below 25 km. The authors should perhaps try showing averaging kernels calculated for a

far finer grid, so that the true vertical resolution of the instrument can be assessed. They could then choose a retrieval grid which matches the achievable resolution better.

Reply: We agree that the possible explanation for the poor precision below 25 km might be the too finer grid resolution. The retrieval grid resolution used in simulation is 1 km below 25 km, 2.5 km below 50 km and 5 km above 50 km. The best retrieval grid resolution needs to be further studied.

A statement has been added in conclusions as follows:
"As the results show that the precision of some products become much poorer suddenly at a height of 25 km, it seems that the retrieval grid resolution does not match the achievable resolution".

Page 23 figure 12: The mixing ratio of CO changes over a very large range. In my experience, the only way to show a vertical profile over the 10 km–90 km range is to use a logarithmic mixing ratio scale.

Reply: Done.

Technical corrections

Page 2 Line 2: "Earth' " should be "Earth's".

Reply: Done.

Page 2 line 28: "Spectrum resolution" should be "spectral resolution".

Reply: Done.

Page 3 line 12: "criterions" should be "criteria". Although there is a trend in modern English away from using Greek or Latin-derived plurals, "criteria" is in very general use, but nobody says "criterions".

Reply: Done.

Page 5, figures 1 – 4: The different lines on these figures can be quite hard to distinguish and to match up with the legend. It would help if the authors were to make the lines slightly thicker and to ensure that they choose strongly-contrasting colours. (They should continue to avoid pure yellow (#ffff00) and pure green (#00ff00) as these colours can be hard to see on a white

ground.) The vertical scale currently goes from 1K to 1000 K, but the data do not cover this entire range. If the software used will permit, the vertical scale should be reduced to cover 2 K to 300K

Reply: Done. All figures have been plotted again.

Page 4 line 16: "as more spectral" should be "as many spectral"

Reply: Done.

Page 4 lines 24–25 and throughout the paper: in LATEX, use a non-breaking thinspace (\,) between a number and its unit in order to avoid a line break at that point. Here, write 635.87\,GHz.

Reply: Done.

Page 8 line 3: T should be in math mode so that it comes out in math italic (T). In LATEX, write T, not T.

Reply: Done.

Diaeresis out of position over de la Nöe's name. Also, "la" does not have a capital letter.

Reply: Done.

Performance Evaluation of THz Atmospheric Limb Sounder (TALIS) of China

Wenyu Wang[1,2], Zhenzhan Wang[1], Yongqiang Duan[1,2]

[1]Key Laboratory of Microwave Remote Sensing, National Space Science Center, Chinese Academy of Sciences, Beijing, China

[2]University of Chinese Academy of Sciences, Beijing, China

Correspondence to: Zhenzhan Wang (wangzhenzhan@mirslab.cn)

Abstract. THz Atmospheric Limb Sounder (TALIS) is a microwave limb sounder being developed for atmospheric high precision observation by the National Space Science Center, Chinese Academy of Sciences (NSSC, CAS). It is designed to measure the temperature and chemical species such as O_3, HCl, ClO, N_2O, NO, NO_2, HOCl, H_2O, HNO_3, HCN, CO, SO_2, BrO, HO_2, H_2CO, CH_3Cl, CH_3OH, and CH_3CN with high vertical resolution from surface to about 100 km to improve our comprehension of atmospheric chemistry and dynamics, and to monitor the man-made pollution in the atmosphere. Four heterodyne radiometers including several FFT spectrometers of 2 GHz bandwidth with 2 MHz resolution are employed to obtain the atmospheric thermal emission in broad spectral regions centred near 118, 190, 240, and 643 GHz. A theoretical simulation is performed to estimate the retrieval precision of the main targets. Single scan measurement and averaged measurement are considered in simulation, respectively. Temperature profile can be obtained with the precision of < 2K for a single scan from 15 to 85 km by using 118 GHz radiometer, and the 240 and 643 GHz radiometer can provide temperature information in the upper troposphere. Chemical species such as H_2O, O_3, HCl show relatively high single scan retrieval precision of 1–20% over most of the useful range and ClO, N_2O, HNO_3 can be retrieved with a precision < 50%. The other species should be retrieved by using averaged measurements because of the weak intensity or low abundance.

1 Introduction

High precision observation of the Earth's atmosphere is essential to the numerical weather prediction and climate change studies. The satellite can provide global coverage atmospheric monitoring in a short time. Instruments such as nadir microwave sounder and infrared sounder have been applied to measure the atmospheric temperature and humidity but with the poor vertical resolution and altitude range (Swadley et al., 2008). Limb sounders can not only provide the temperature profile with better vertical resolution but gather information on chemical composition in a wide altitude range. In the terahertz domain, the measurement performances are independent of the day-night cycle. Microwave limb sounding is a particularly useful technique in detecting stratospheric and mesospheric temperature and chemistry, and also has large potential for global wind measurement in the middle and upper atmosphere (Wu et al., 2008; Baron et al., 2013).

A few instruments have been launched in recent twenty years, their observation data have offered a better understanding of the physical and chemical processes in the Earth's atmosphere. The first instrument applying the microwave limb sounding technique from space was the Microwave Limb Sounder (MLS) onboard the Upper Atmosphere Research Satellite (UARS) launched in 1991. The sounder offered unique information of temperature/pressure, O_3, H_2O, ClO, and additional data products including SO_2, HNO_3, and CH_3CN (Waters et al., 1993). The Sub-Millimetre Radiometer (SMR) onboard the Odin satellite launched in February 2001 was the first radiometer to employ sub-millimetre in limb sounding. Various target species such as O_3, ClO, N_2O, HNO_3, H_2O, CO, NO, as well as isotopes of H_2O, O_3, and ice cloud have been detected (Murtagh et al., 2002; Urban et al., 2005; Eriksson et al., 2007). EOS MLS, the follow-on of UARS MLS onboard the Aura satellite launched in July 2004 gave successful observations of OH, HO_2, H_2O, O_3, HCl, ClO, HOCl, BrO, HNO_3, N_2O, CO, HCN, CH_3CN, SO_2, ice cloud, and wind (Waters et al., 2004; Waters et al., 2006; Wu et al., 2008; Livesey et al., 2013). The Superconducting Submillimeter-wave Limb-Emission Sounder (SMILES) onboard the Japanese Experiment Module (JEM) of the International Space Station (ISS) launched in September 2009 (Kikuchi et al., 2010). SMILES was equipped with 4K cooled Superconductor–Insulator–Superconductor (SIS) mixers to reduce the system noise temperature so that the sensitivity of the SMILES was higher than that of other similar sensors such as MLS and SMR (Takahashi et al., 2010; Baron et al., 2011). Currently, several new instruments are being developed. Stratospheric Inferred Winds (SIW) is a Swedish mini sub-millimetre limb sounder for measuring wind, temperature, and molecules in the stratosphere. It can provide horizontal wind vectors within 30–90 km, as well as the profiles of temperature, O_3, H_2O and other abundant chemical species (Baron et al., 2018). SIW is designed for small satellites and will be launched as early as 2020–2022. In addition, the follow-on of SMILES, SMILES-2, is being studied for measuring the whole vertical range of 15−180 km with low noise (Ochiai et al., 2017).

THz Atmospheric Limb Sounder (TALIS) is the pre-research project of civil aerospace technology proposed by China National Space Administration (CNSA). TALIS is being designed at National Space Science Center, the Chinese Academy of Sciences (NSSC, CAS) for high precision measurement of atmospheric temperature and key chemical species. It has four microwave radiometers in the frequency bands of 118, 190, 240, and 643 GHz which are similar to EOS MLS. TALIS mission objectives are to provide the information for research on the dynamics and the chemistry of the middle and upper atmosphere by measuring the volume mixing ratio (VMR) profile of the chemical species and other atmospheric condition such as cirrus with much finer spectral resolution. The pre-research will be completed in 2020 and a prototype will be tested. The satellite mission equipped with TALIS will be proposed around 2021.

In this paper, we present a simulation study on precision estimates for the geophysical parameters measured by TALIS. The outline of the present study is as follows: Section 2 describes the instrument characteristics and spectral bands. The retrieval method and the simulation result are discussed in Sects. 3 and 4, respectively. The final section gives a conclusion about the performance and future works.

2 Instrument overview

2.1 Instrument characteristics

The TALIS payload (Fig. 1) and its proposed scan characteristics are summarized in Table 1. The instrument will be set at a sun-synchronous orbit at a normal altitude of 600 km. The offset parabolic antenna is made of a single reflector with 1.6 m projective aperture and four independent feeds. The layout of four discrete feeds is shown in Fig. 2. Compared with the quasi-optical separation layout (such as MLS), this strategy is easier and has higher observation precision. But it will lead to an observed difference of about 20 km between the four radiometers. The widths of the field of view (FOV) at the tangent point are about 5.5, 3.8, 3.3, and 0.96 km respectively. The two-point calibration method is adopted by TALIS, and an extra calibration target is set at the bottom of the antenna. The extra target can be used to improve the calibration precision and evaluate the antenna effect and nonlinearity. At the beginning of the scan, TALIS will view the hot target (ambient temperature) and the extra target (lower temperature) in 3 s, and then it will scan the limb from 0 to 100 km vertically and obtain the spectra every 1 km with an integration time of 0.1 s, finally, it views the cold space at 200 km in 5 s. The process of retrace is the same (also record data) and giving a total period of about 36 s.

TALIS has four radiometers which cover the significant thermal emission spectra in the 118, 190, 240, and 643 GHz regions (see Table 2). Single-sideband (SSB) can keep the complete spectral lines while double-sideband (DSB) can cover more spectral lines because of the image band. Thus, all the radiometers of TALIS will operate in the double-sideband mode except the 118 GHz radiometer. Eleven FFT spectrometers of 2 GHz bandwidth with 2 MHz resolution will be used in TALIS. The bands and system noise temperature for each radiometer are shown in Table 2.

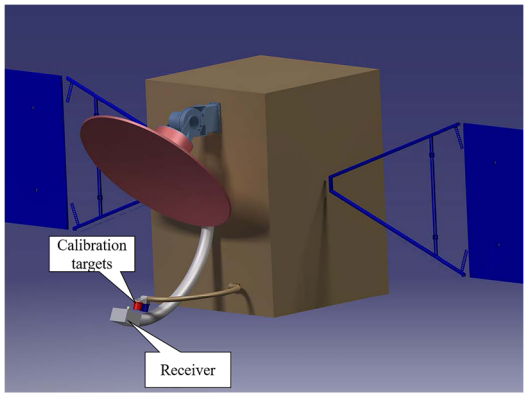

Figure 1. The schematic diagram of TALIS payload

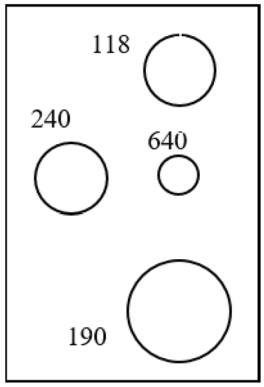

Figure 2. The layout of the four antenna feeds

Table 1. Characteristics of the TALIS payload

Satellite altitude	600 km
Scan altitude	0–100 km
LOS nadir angle	66.07–68.17° （2.1° ）
Scan velocity	0.21° s^{-1} (36 s $scan^{-1}$)
Spectrum integration time	0.1 s (1 km)
Antenna size	1.6 m

Antenna vertical FOV	5.5, 3.8, 3.3, 0.96 km
Spectrometer Bandwidth	2 GHz
Spectrometer resolution	2 MHz
LO frequency	120, 190.1, 239.66, 642.87 GHz

Table 2. Spectral bands and Tsys of TALIS

Radiometer	TALIS (GHz)	Tsys* for TALIS	Tsys for MLS	Radiometer	TALIS (GHz)	Tsys for TALIS	Tsys for MLS
118 GHz	117.75–119.75	800 K	1200 K	240 GHz	229.66–231.66 247.66–249.66	1000 K	1200–1600 K
190 GHz	175.5–177.5 202.7–204.7	1000 K	900–1100 K		232.16–234.16 245.16–247.16		
	178.9–180.9 199.3–201.3				234.66–236.66 242.66–244.66		
	183.0–185.0 195.2–197.2			643 GHz	624.47–626.47 659.27–661.27	3000 K	4000–4400 K
					627.37–629.37 656.37–658.37		
					632.37–634.37 651.37–653.37		
					634.87–636.87 648.87–650.87		

* This is a single-sideband value for 118 GHz radiometer, and double-sideband value for other radiometers.

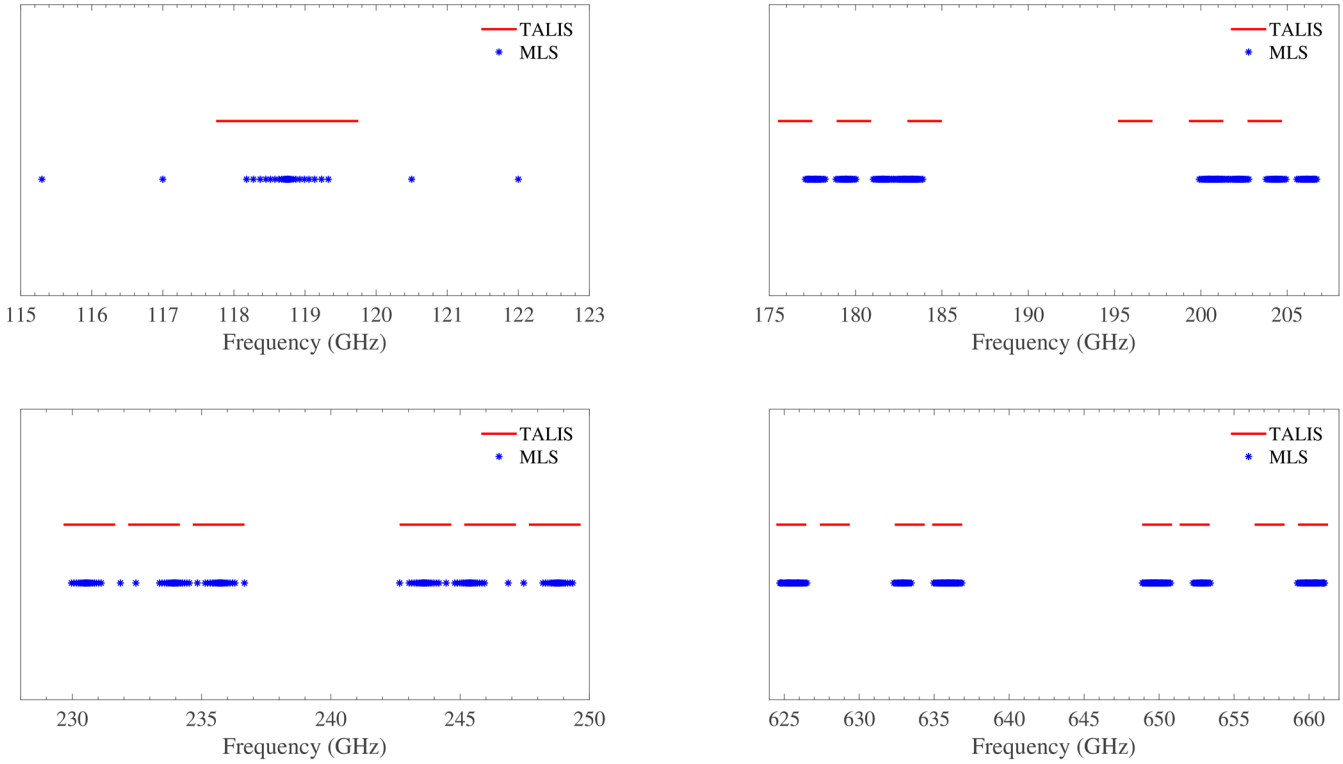

Figure 3. Spectral bands of EOS MLS and TALIS radiometers.

2.2 Spectral bands

The spectral bands of TALIS are selected with the following criteria: (1) maximizing the number of species which will exert a strong influence on atmospheric chemistry and dynamics, (2) necessary space between the passband, (3) trade-off between realizable bandwidth and resolution. TALIS covers most spectral bands of EOS MLS and extends them (see Fig 3), but lack the 2.4 THz band. The broader bandwidth and the finer resolution of TALIS can provide higher retrieval precision and effective altitude range compared with EOS MLS. More chemical species can be measured by TALIS, such as NO_2, NO, and SO_2 (normal concentration).

The 118 GHz radiometer, covering the strong O_2 line at 118.75 GHz, is used to measure the atmospheric temperature and tangent pressure. Since there are few meteorological data set about the temperature above the middle atmosphere with good vertical resolution, it is necessary to measure the temperature profile with wide altitude range, good vertical resolution, and high precision. Other information such as ice cloud can be treated as additional measurement. Figure 4 gives an overview of the 118 GHz spectral band.

The 190 GHz radiometer is mainly designed to cover the 183.31 GHz H_2O line. Monitoring water vapour is important for understanding the mechanisms that humidity feedback on climate, and is essential for improving the accuracy of the weather forecast. Other chemical species such as N_2O, ClO, O_3, and HCN are also included in 190 GHz bands (see Fig. 5).

The main objective of the 240 GHz radiometer is to measure the CO at 230.54 GHz and the strong O_3 lines in a wide spectral band where upper tropospheric O_3 can be obtained with high precision because of the weak water vapour continuum absorption. In addition, the 233.95 GHz O_2 line will be used to measure temperature and tangent pressure together with 118.75 GHz line. SO_2 is an important pollutant in the Earth' atmosphere and will give rise to acid rain. There is no obvious SO_2 emission with the standard profile present in the passband of 240 GHz radiometer. The only SO_2 which is observable by MLS comes from volcanic eruptions. MLS demonstrated that SO_2 can be measured by 190 GHz, 240GHz, and 640 GHz radiometer, but only 240 GHz SO_2 product is recommended for general use. (Pumphrey et al., 2015). The wide and strong lines of HNO_3 can be used to retrieve profile well. NO_2 is a unique species not covered by EOS MLS, and TALIS's wider bandwidth and finer resolution have the potential ability to measure it. The spectra of 240 GHz radiometer are depicted in Fig. 6.

The 643 GHz radiometer is designed to cover as many spectral lines as possible, thus about 17 species are included. The spectral lines covering O_3, HCl, ClO, N_2O, O_2, and H_2O are clearly visible (Fig. 7), and other lines which are relatively weak such as NO, HNO_3, CO, SO_2, BrO, HO_2, H_2CO, HOCl, and CH_3Cl, can also be used. The O_2 line at 627.75 GHz and the H_2O line at 657.9 GHz have the potential to be used as supplements to 118 and 190 GHz radiometers. O_3 is the major species in the stratosphere and mesosphere, which is quite important in atmospheric radiation transfer. Using the high sensitivity lines in the 643 GHz bands, one can measure O_3 with high precision (Takahashi et al., 2011; Kasai et al., 2013). The only lines of HCl below 1 THz are in the 625 GHz frequency band, thus HCl can be measured by 643 GHz radiometer. ClO is a key catalyst for ozone loss and the 649.45 GHz line is suitable for ClO observation with good precision (Santee et al., 2008;

Sato et al., 2012). The HOCl, which will affect stratospheric chlorine budget, has distinct lines above 600 GHz, and the 635.87 GHz line has been pointed out to be the best line for observation (Urban, 2003). Both 649.701 and 660.486 GHz lines can be used to measure the hydroperoxyl radical HO_2, which will contribute to the catalytic ozone chemistry in the upper stratosphere and mesosphere (Millán et al., 2015). Since ClO, HO_2, and HOCl all can be measured, the reaction rate of ClO and HO_2 to form HOCl in the atmosphere can be determined (Johnson et al., 1995). N_2O can be measured at 652.834 GHz, which has been validated by MLS (Lambert et al., 2008). NO has two weak signals at 651.45 and 651.75 GHz which can be used to measure the abundance. HNO_3 can be measured using 650 GHz bands. Measuring these nitrogen species will help researchers to understand the chemistry and dynamics of the atmosphere better. The BrO, which plays an important role in the depletion of ozone, can be measured using 624.768 and 650.179 GHz lines. Because of the low abundance of BrO, measurements must be significantly averaged in order to get reliable results (Millán et al., 2012). CO and H_2CO are the major species in the CH_4 oxidation to CO_2 and H_2O in the stratosphere and mesosphere (Suzuki et al., 2015). The major spectral line of CO used by MLS is at 230.538 GHz, however, the 661.07 GHz line can also provide information (Livesey et al., 2008). H_2CO has a line at 656.45 GHz, but the signal is very weak. The SO_2 lines in the 660 GHz band have the potential to detect the background levels of SO_2. CH_3Cl can be measured in the 649 GHz band near the line of ClO. MLS measured CH_3OH and CH_3CN in the troposphere and lower stratosphere by 625 GHz spectrometer (Pumphrey et al., 2011).

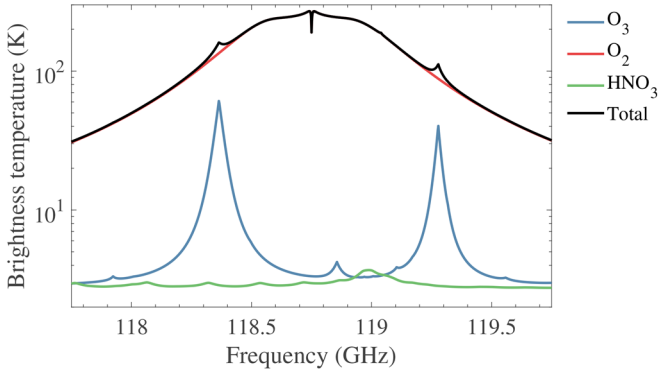

Figure 4. Contributions of the main target chemical species to the 118 GHz spectrum. The brightness temperature is measured from single sideband radiometer. The tangent height is 30 km.

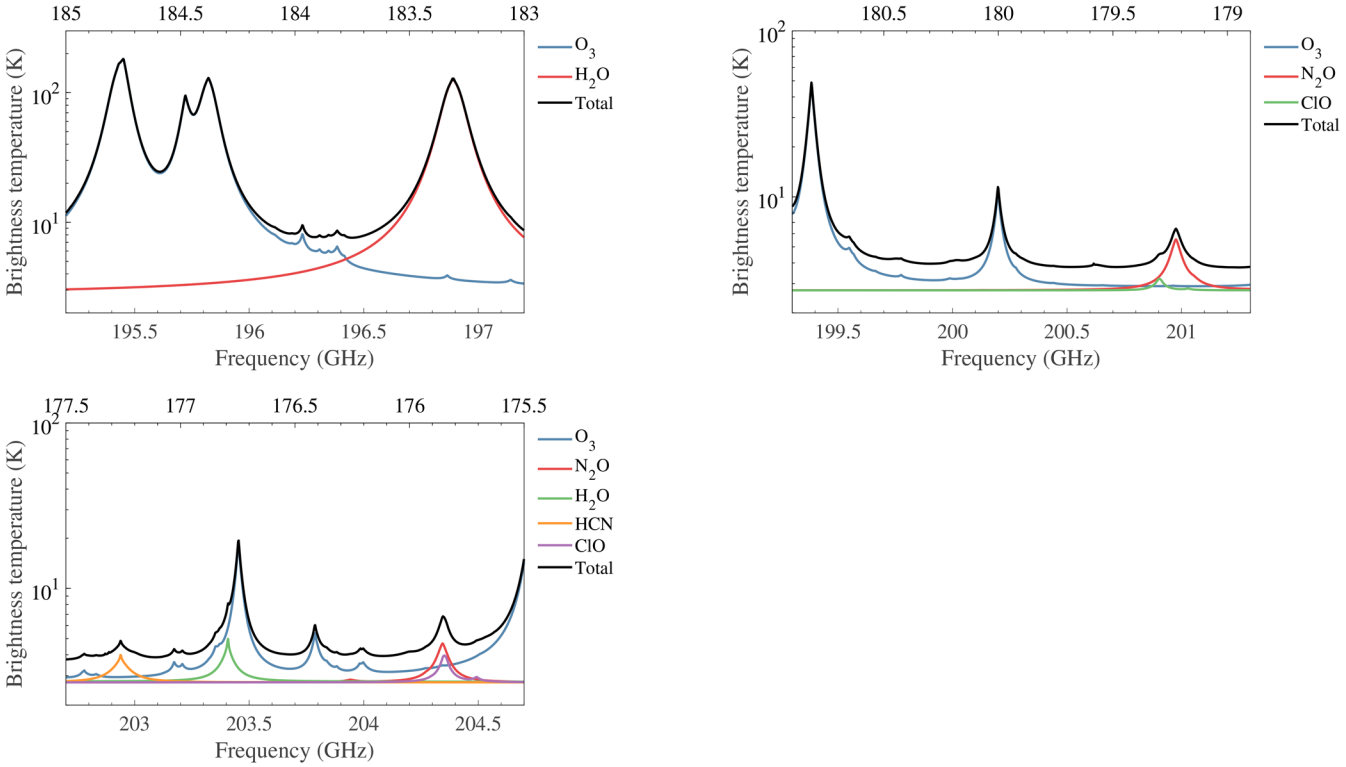

Figure 5. Contributions of the main target chemical species to the 190 GHz spectra. The brightness temperature is measured from double sideband radiometer. The tangent height is 30 km. The top axis represents the lower sideband frequencies and the bottom axis represents the upper sideband frequencies. Each panel represents a single spectrometer.

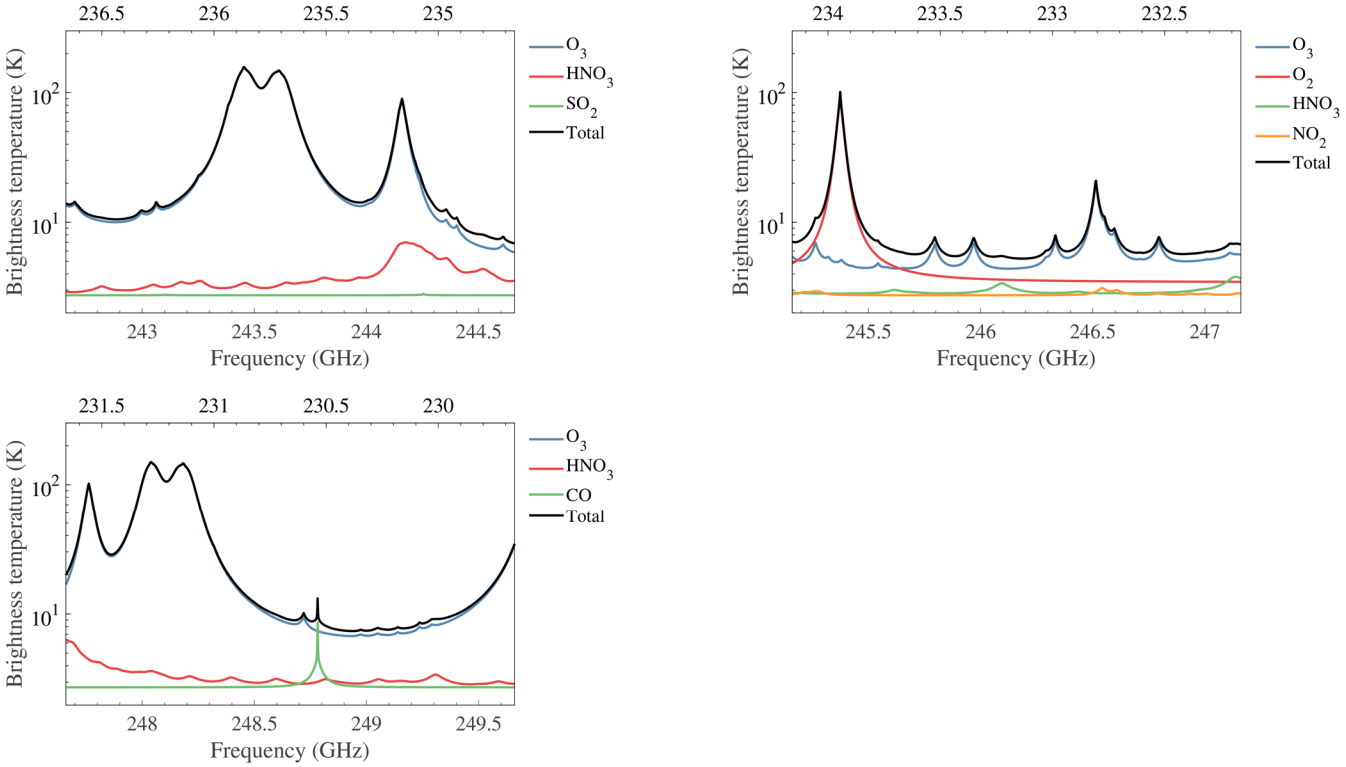

Figure 6. Contributions of the main target chemical species to the 240 GHz spectra. The brightness temperature is measured from double sideband radiometer. The tangent height is 30 km. The top axis represents the lower sideband frequencies and the bottom axis represents the upper sideband frequencies. Each panel represents a single spectrometer.

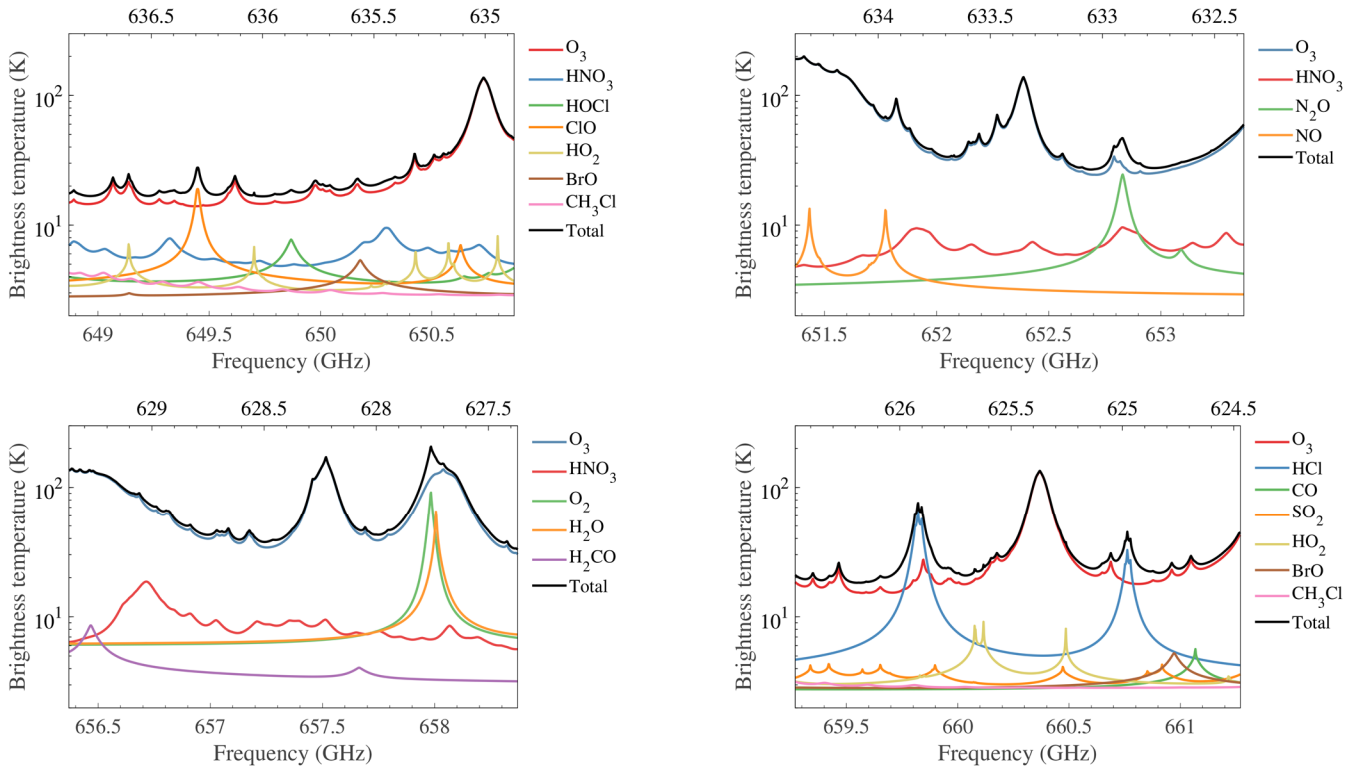

Figure 7. Contributions of the main target chemical species to the 643 GHz spectra. The brightness temperature is measured from double sideband radiometer. The tangent height is 30 km. The top axis represents the lower sideband frequencies and the bottom axis represents the upper sideband frequencies. Each panel represents a single spectrometer.

3 Retrieval methodology

3.1 Forward model

The retrieval of data measured by microwave limb sounder requires the accurate simulation of the observed thermal emission spectra. The forward model is a mathematical tool used to describe the radiative transfer, spectroscopy, and instrumental characteristics. The output of the forward model is the convolution of atmospheric radiation and instrument response.

Radiative transfer describes the emission, propagation, scattering, and absorption of electromagnetic radiation (Mätzler., 2006). Scattering usually can be neglected above the upper troposphere because of the cloud free. In this way and assuming Local Thermodynamic Equilibrium (LTE), the formal solution of the radiative transfer equation is defined by

$$I_v(S_2) = I_v(S_1)e^{-\tau_{v(S_1,S_2)}} + \int_{S_1}^{S_2} \alpha_v(s)B_v(T)e^{-\tau_{v(S,S_2)}}ds, \quad (1)$$

where I_v is the radiance at frequency v reaching the sensor, α is the absorption coefficient and τ is the opacity or optical thickness. B_v stands for the atmospheric emission which is given by Planck function describing the radiation of a black-body at temperature T and frequency v per unit solid angle, unit frequency interval and unit emitting surface (Urban et al., 2004):

$$B_v(T) = \frac{2hv^3}{c^2}\frac{1}{e^{hv/k_BT}-1}, \quad (2)$$

where h is the Planck constant, c is the speed of light, k_B denotes Boltzmann constant.

Spectroscopy is the method to calculate the absorption coefficient which requires pressure, temperature, and the species concentrations along the line of sight. The basic expression can be written as:

$$\alpha(v) = nS(T)F(v), \quad (3)$$

where S is called the line strength, F means the line shape function, and n is the number density of the absorber.

Sensor characteristics also have to be taken into account by the forward model, including the antenna field-of-view, the sideband folding, and the spectrometer channel response (Eriksson et al., 2006).

Firstly, the radiance which encounters the antenna response could be expressed by the integration:

$$I_v^a = \int_\Omega I_v(\Omega)W_v^a(\Omega)d\Omega, \quad (4)$$

where W_v^a is the normalized antenna response function. Normally, the variation of I_v in azimuth angle dimension can be neglected or calculated before-hand. Secondly, a heterodyne mixer needs to convert the signals to intermediate frequency, which will lead to a consequence that the lower and upper sideband are folded. The apparent intensity after the mixer can be modelled as:

$$I_v^{if} = \frac{W_v^s(v)I_v^a + W_v^s(v')I_{v'}^a}{W_v^s(v)+W_v^s(v')}, \quad (5)$$

where W_v^s means the sideband response. At last, the final signal will be recorded by spectrometers, which can be described in a similar way as the antenna response:

$$I^c = \int_v I_v^{if} W_v^c(v)dv. \quad (6)$$

Here W_v^c means the normalized channel response, and the radiance is denoted I^c.

The measured radiance is transformed to brightness temperatures using the Planck's function.

3.2 Retrieval algorithm

Optimal estimation method (OEM) is the most common method used in atmospheric sounding for retrieving vertical profiles of chemistry species (Rodgers, 2000).

In OEM theory, a predicted noisy measurement $\hat{\boldsymbol{y}}$ can be expressed by a forward model $\boldsymbol{F}$ with an unknow atmospheric state $\boldsymbol{x}$ and the system noise ϵ_y according to:

$$\hat{\boldsymbol{y}} = \boldsymbol{F}(\boldsymbol{x}, \boldsymbol{b}) + \epsilon_y. \quad (7)$$

The noiseless predicted radiance $F(x, b)$ are compared with the observed radiance y so that the unknow state which minimize the cost function χ^2 could be found. The cost function is given by:

$$\chi^2 = [\boldsymbol{y} - \boldsymbol{F}(\boldsymbol{x}, \boldsymbol{b})]^T \boldsymbol{S}_y^{-1} [\boldsymbol{y} - \boldsymbol{F}(\boldsymbol{x}, \boldsymbol{b})] + [\boldsymbol{x} - \boldsymbol{x}_a]^T \boldsymbol{S}_a^{-1} [\boldsymbol{x} - \boldsymbol{x}_a], \quad (8)$$

where x_a is a priori state vector, $\boldsymbol{S}_a$ and $\boldsymbol{S}_y$ stand for the covariance matrices representing the natural variability of the state vector and the measurement error vector, respectively. Assuming there is no correlation between channels, the off-diagonal elements of $\boldsymbol{S}_y$ are zero and the diagonal elements are set to the square of the system noise. Usually, a simple formula can be used to determine the SSB radiometric noise standard deviation:

$$\epsilon = \frac{T_{sys}}{\sqrt{\beta\, d\tau}}, \quad (9)$$

where T_{sys} is the system noise temperature which is the sum of receiver noise temperature and the atmosphere temperature received by the antenna, β is the noise equivalent bandwidth and $d\tau$ is the integration time for measuring a single spectrum. When it comes to DSB radiometer, the ϵ need to be divided by $\sqrt{2}$. The diagonal elements of the S_a specify a priori variance and the off-diagonal terms are used to describe correlations between adjacent elements in order to make the retrieved profile smoother.

Finally, the Levenberg–Marquardt method which is the modification of the Gauss-Newton iterative is used to solve the nonlinear problem. The solution is given by

$$\boldsymbol{x}_{i+1} = \boldsymbol{x}_i + \left[(\boldsymbol{I} + \gamma)\boldsymbol{S}_a^{-1} + \boldsymbol{K}_{xi}^T \boldsymbol{S}_y^{-1} \boldsymbol{K}_i\right]^{-1} \left\{\boldsymbol{K}_{xi}^T \boldsymbol{S}_y^{-1} [\boldsymbol{y} - \boldsymbol{F}(\boldsymbol{x}_i)] - \boldsymbol{S}_a^{-1} (\boldsymbol{x}_i - \boldsymbol{x}_a)\right\}, \quad (10)$$

where γ denotes the Levenberg–Marquardt parameter, and $\boldsymbol{K}_{xi}$ represents the weighting function matrix (Jacobian).

The OEM method provides an approach to describe the retrieval error completely. The averaging kernel matrix $\boldsymbol{A}$, which represent the sensitivity of the retrieved state to the true state, is written as:

$$\boldsymbol{A} = \boldsymbol{G}_y \boldsymbol{K}_x = \frac{\partial \hat{\boldsymbol{x}}}{\partial \boldsymbol{x}}, \quad (11)$$

where the G_y is the contribution matrix, which express the sensitivity of the retrieved state to the measurement:

$$\boldsymbol{G}_y = \frac{\partial \hat{\boldsymbol{x}}}{\partial \boldsymbol{y}} = \left(\boldsymbol{K}_x^T \boldsymbol{S}_y \boldsymbol{K}_x + \boldsymbol{S}_a^{-1}\right)^{-1} \boldsymbol{K}_x^T \boldsymbol{S}_y^{-1}. \quad (12)$$

The retrieval resolution can be estimated from the full width at half-maximum (FWHM) of the averaging kernel (Marks and Rodgers, 1993).

There is another useful variable defined as measurement response, which represents the true state contribution in the retrieval (Baron et al., 2002):

$$W(i) = \sum_j |A(i,j)|. \quad (13)$$

The ideal measurement response should be near 1. In practice, reliable range of a retrieval is usually characterised by $|W - 1| < 0.2$.

The total retrieval error can be described by three covariance matrices, the smoothing error covariance matrix which is from the need of a priori information:

$$\boldsymbol{S}_n = (\boldsymbol{A} - \boldsymbol{I})\boldsymbol{S}_a(\boldsymbol{A} - \boldsymbol{I})^T, \quad (14)$$

the measurement error covariance matrix due to the measurement noise:

$$\boldsymbol{S}_m = \boldsymbol{G}_y \boldsymbol{S}_y \boldsymbol{G}_y{}^T, \tag{15}$$

and the model parameter error covariance matrix introduced by the uncertainties in the forward model:

$$\boldsymbol{S}_s = \boldsymbol{G}_y \boldsymbol{K}_b \boldsymbol{S}_b \boldsymbol{G}_y \boldsymbol{K}_b{}^T. \tag{16}$$

4 Measurement performance

4.1 Simulation setup

The objective of the simulation is to evaluate the observation performance of TALIS. In this simulation, the forward model Atmospheric Radiative Transfer Simulator (ARTS 2.3) and its corresponding retrieval tool Qpack2 are used (Eriksson et al., 2005; Eriksson et al., 2011). The instrumental setup follows the characteristics of TALIS described in Table 1 and Table 2. The ideal rectangle channel response function is used. The simulation antenna patterns of the four radiometers are shown in Fig. 8. As the antenna calibration can be done by a linear function, it has no impact on the following simulation, so antenna pattern is not added in simulation below.

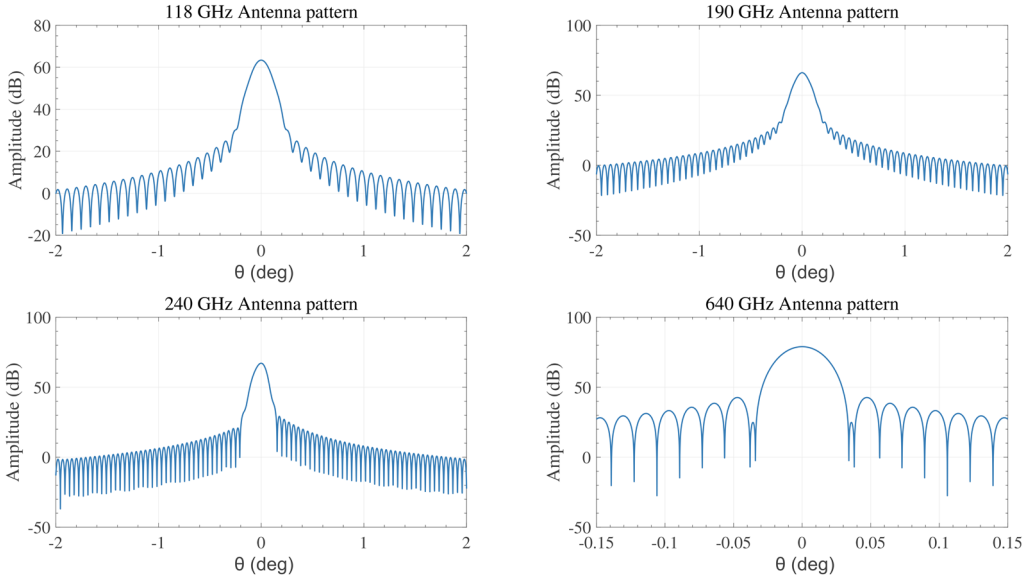

Figure 8. The antenna patterns of TALIS.

In this simulation, the scan altitude range is from 10 to 95 km and the spectra are obtained every 2.5 km. As the effective FOV of TALIS are similar to MLS, we use 2.5 km as the vertical resolution. It is the trade-off between the step of efficient limb observation and the optimum information can be obtained (Livesey and Snyder, 2004).

A mid-latitude summer atmospheric condition (profiles of BrO and HO_2 are from MLS L3 data) is chosen to perform the simulation. The scattering from tropospheric clouds, refraction, and Zeeman effect are not considered because of the large computational complexity. A spectroscopic line parameters catalogue created with the data taken from JPL catalogue (Pickett et al., 1998), HITRAN database (Rothman et al., 2013), and Perrin catalogue (Perrin et al., 2005) is used for line-by-

line absorption calculation. The measurement covariance matrix is set diagonal as described in Sect.3 in order to reduce the computing time. 100% of a typical profile is used to build the a priori covariance matrix with 3 km vertical correlation between the adjacent pressure levels by a parametric Gaussian function. The true profiles are defined with a vertical resolution of 0.5 km. The true species profiles are multiplied by a factor of 1.1 to be the a priori profiles, and the true temperature profile is added a 5 K offset to be the a priori profile. The retrieval grid resolution is 1 km below 25 km, 2.5 km below 50 km, and 5 km above 50 km.

The expected 1σ noise is calculated by Eq. (10), and thus the noise is assumed to be 2 K, 1.7 K, 1.7 K, and 5 K, respectively. The species such as BrO and HO_2 which emission radiances are small compared with the system noise must be averaged to increase the precision. Here the lower noise (1σ noise multiply a factor of 0.1) is used to represent the averaged production.

4.2 Comparison of TALIS and EOS MLS

As discussed in section 2.2, TALIS has similar bands to EOS MLS. The major difference between these two instruments is the spectrometers used in limb sounding. A simulation is performed to compare the performance of the main products between TALIS FFT spectrometer and EOS MLS 'Standard' 25-channel spectrometer. Figure 9 to 11 show the retrieval products of TALIS and MLS, all the factors are identical except the spectrometer.

According to the simulation results, TALIS can do a better job than EOS MLS because of the wider bandwidth and finer resolution. Temperature precision of TALIS is improved 1–2 K compared with EOS MLS and the vertical resolution is improved about 2 km. H_2O precision is improved about 2–10 %. O_3 precision is improved about 2–20 % and retrieved well in the mesosphere.

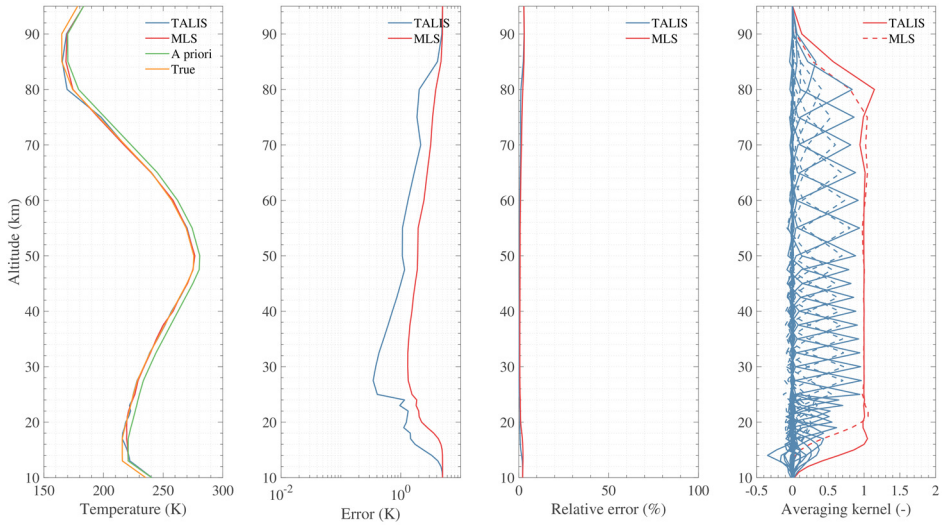

Figure 9. Temperature product comparison between TALIS FFT spectrometer and MLS 'Standard' spectrometer using 118.75 GHz line. All other factors are identical.

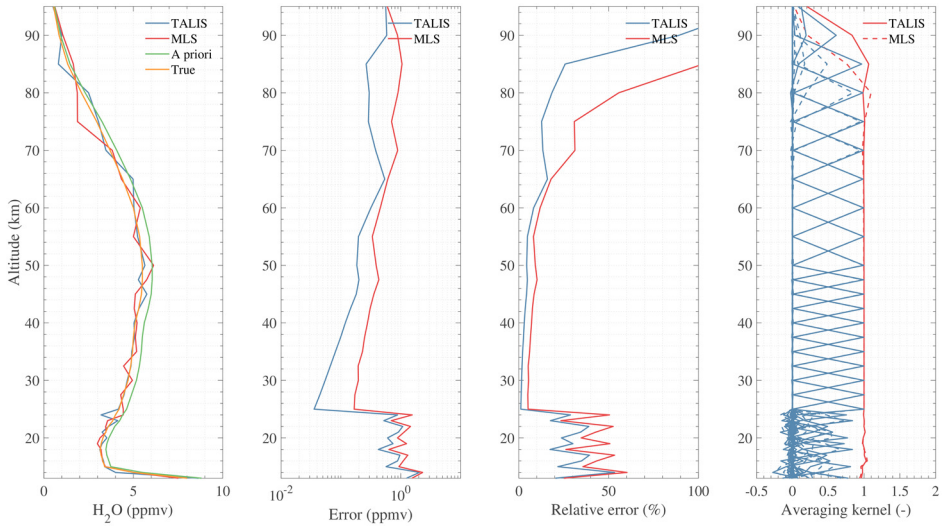

Figure 10. H_2O product comparison between TALIS FFT spectrometer and MLS 'Standard' spectrometer using 183.31 GHz line. All other factors are identical.

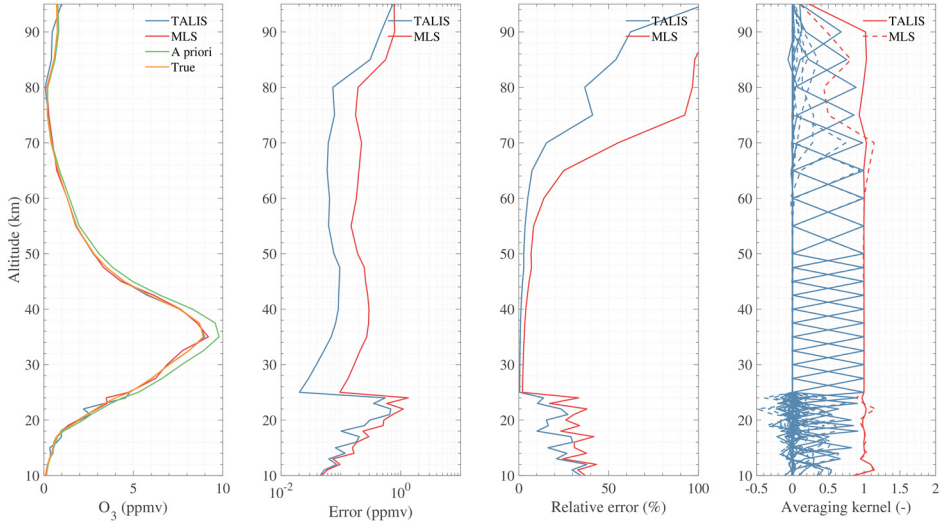

Figure 11. O_3 product comparison between TALIS FFT spectrometer and MLS 'Standard' spectrometer using 235.71 GHz line. All other factors are identical.

4.3 Retrieval precision

Since the simulation has been performed, an evaluation of the retrieval precision on the target species of TALIS is made. Retrieval profile, a priori profile, and true profile are all plotted in Figs. 12 to 28. The precision (square root of diagonal elements of the error covariance matrix) is given for a single scan and averaged measurement respectively, and the relative error is also provided. Auxiliary information about averaging kernel function and measurement response are also included. Results are discussed in details in the followings.

4.3.1 High precision products

Temperature, H_2O, O_3, HNO_3, HCl, N_2O, and ClO are treated as high precision products because of the good precision for a single scan measurement. These products can be used in scientific research directly.

Atmospheric temperature is the most important parameter that can be retrieved with high signal-noise ratio in lower frequency or good vertical resolution in high frequency by using O_2 lines. TALIS will use 118 GHz radiometer to detect atmospheric temperature profile, with 240 and 643 GHz radiometers worked as supplement products. Results are shown in Fig. 12, the sensitivity is significantly high at the 118 GHz band. Single scan precision is < 1K from 25 to 45 km and < 2K at other useful range. The retrieval vertical resolution is 2.5 km below 50 km and 5–6 km from 50 to 80 km. The precision of averaged measurement will be < 1K from 15 to 85 km.

'Wide' filters of MLS make measurements extending down into the troposphere, and TALIS is lack of the information. However, the retrieval precision of 240 GHz band is better in the upper troposphere and the 240 GHz product can compensate for the loss of information. Result of 643 GHz band looks similar to that of 240 GHz band.

Once the temperature profile is retrieved, the pressure profile can be calculated from the hydrostatic equilibrium equation using a known pressure and temperature at a reference tangent point. The pressure profile is not a direct product and is not shown here.

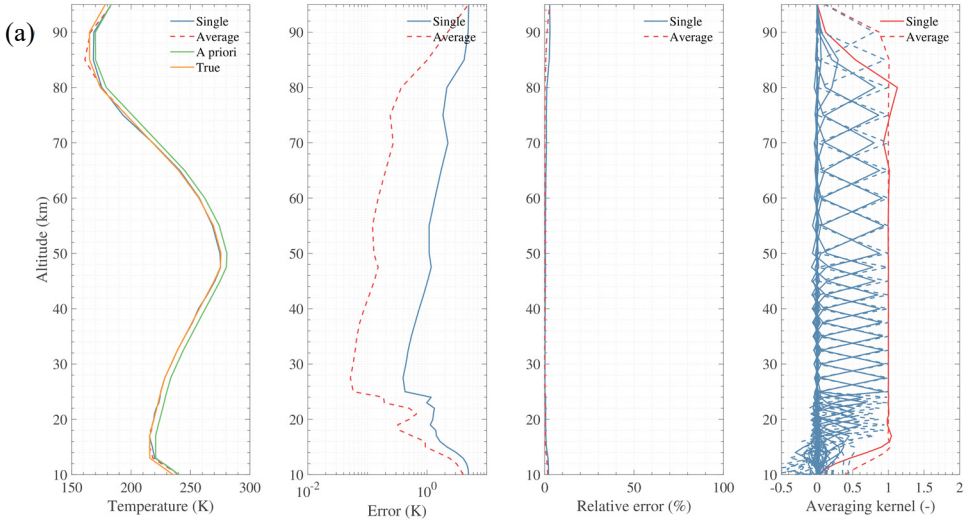

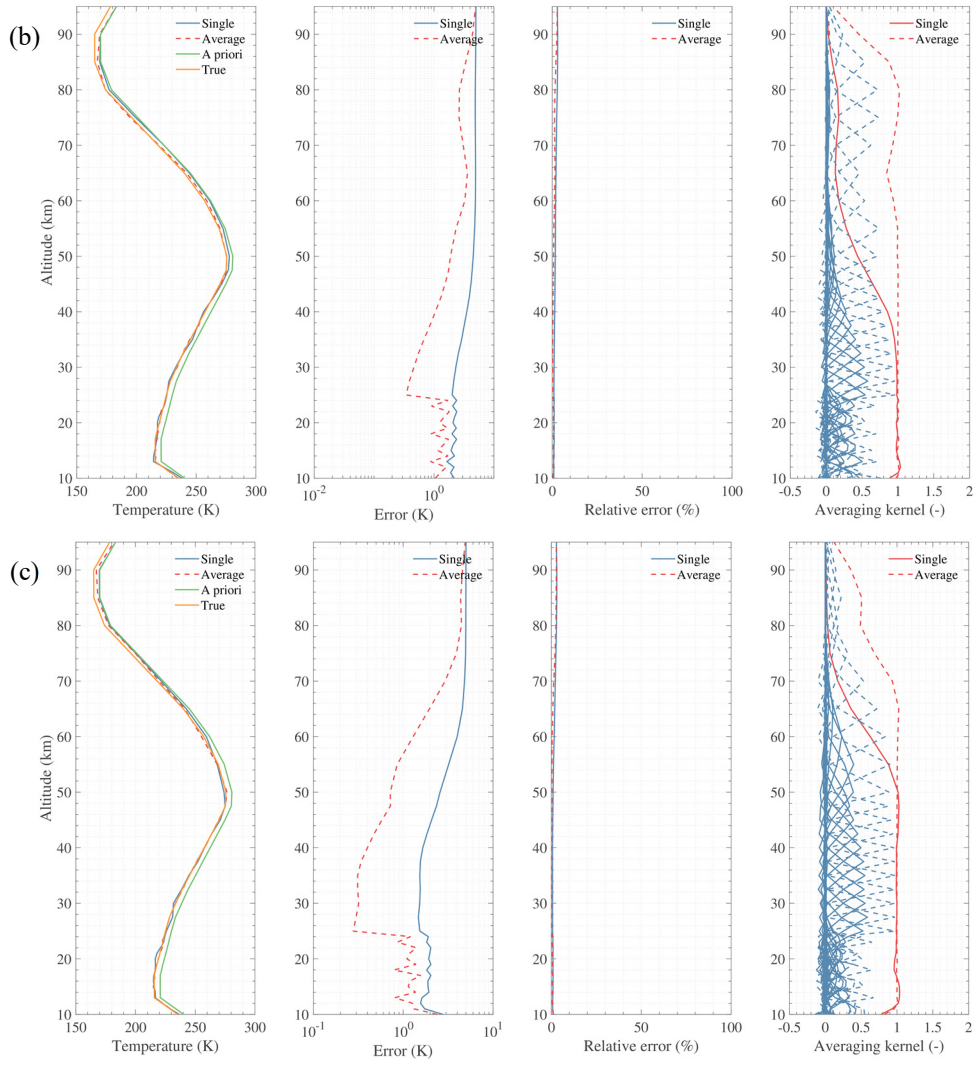

Figure 12. Simulation results of temperature retrieval using 118.75 (a), 233.95 (b), and 627.75 GHz (c) lines.

The H_2O profile, another key parameter, can be measured by 190 and 643 GHz radiometers. The 183.31 GHz line is generally used by humidity sounder to detect water vapour with high precision. Figure 13 shows the retrieval precision will be < 10% from 25 to 75 km by 190 GHz single scan measurement with the vertical resolution of 2.5–5 km. Averaged measurement has the retrieval precision < 1% at 25–80 km, < 20% at other effective altitudes. The profile can also be retrieved by 643 GHz radiometer with less precision.

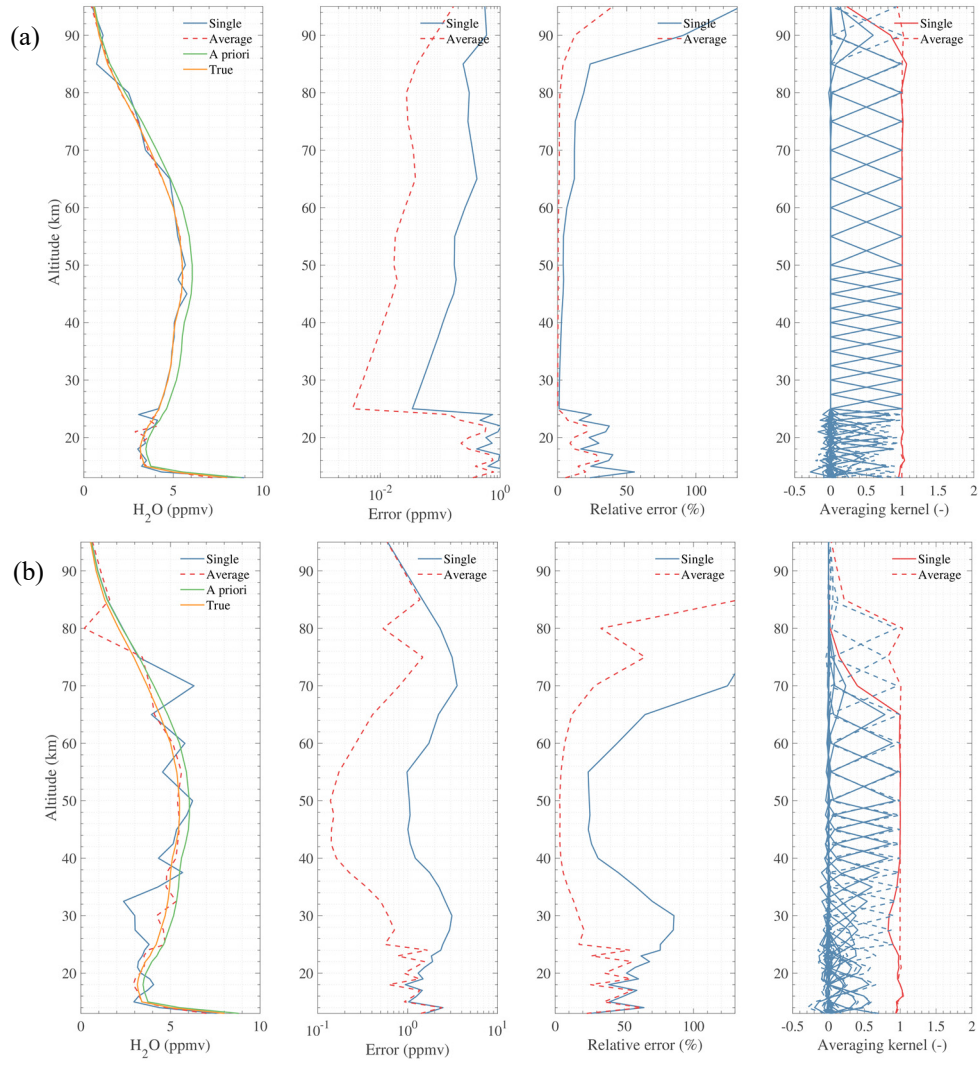

Figure 13. Simulation results of H_2O retrieval using 183.31 (a) and 657.9 GHz (b) lines.

O_3 has quite strong intensity in most spectral regions of TALIS. All the radiometers except 118 GHz can be used to observe this gas which is important for energy balance (Fig. 14). The 240 GHz radiometer which covers the 235.7 GHz line has the highest O_3 sensitivity. The profile can be retrieved with a single scan precision < 5% from 25 to 60 km and the vertical resolution is 2.5 km. The vertical resolution will degrade to 5–8 km for altitudes higher than 60 km. By averaging the measurements, the precision will be < 1% at 25–65 km. The other two bands show good performance from 25 to 60 km with a single scan precision < 5%.

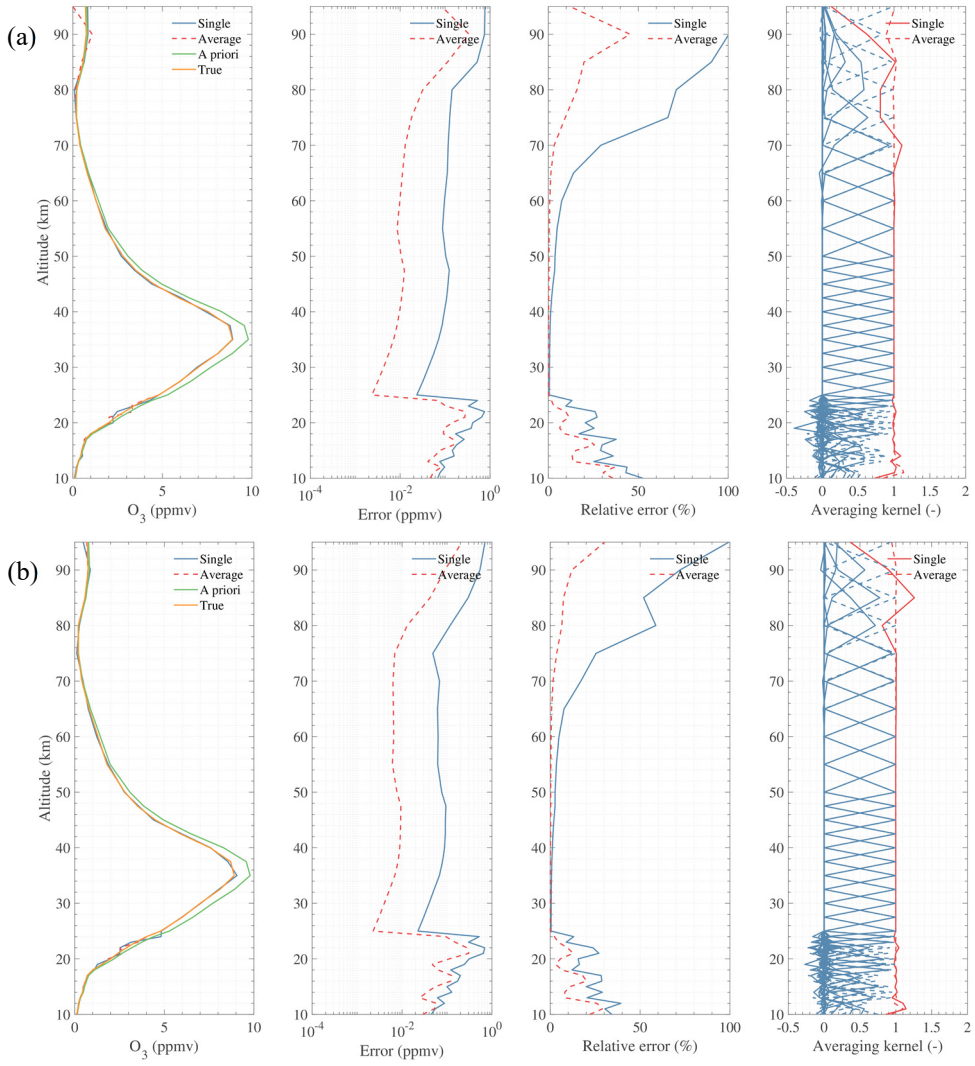
(a)
Single
Average
A priori
True
Altitude (km)
O3 (ppmv)
Error (ppmv)
Relative error (%)
Averaging kernel (-)
(b)
Single
Average
A priori
True
Altitude (km)
O3 (ppmv)
Error (ppmv)
Relative error (%)
Averaging kernel (-)

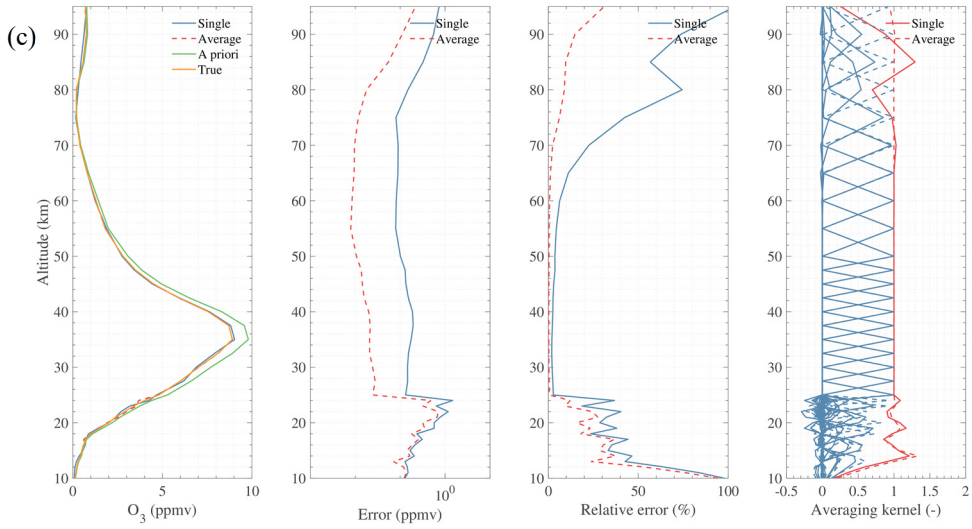

Figure 14. Simulation results of O_3 retrieval using 190 (a), 235.7 (b), and 657.5 GHz (c) lines.

HNO_3 is a common species in the stratosphere and has relatively strong lines at 240 and 643 GHz bands. Figure 15 shows the results of HNO_3 retrieval. The 240 GHz radiometer can measure HNO_3 at 25–35 km altitude range with a single scan precision < 30% and the vertical resolution is 2.5–5 km through most of the useful range. Averaging the measurements can improve the retrieval with a precision < 10% from 25 to 35 km. The 643 GHz signal is stronger than that in the 240 GHz band, but it is strongly absorbed by O_3 below about 30 km. However, after averaging the measurements, information can be retrieved between 25 and 70 km with a precision better than 50%.

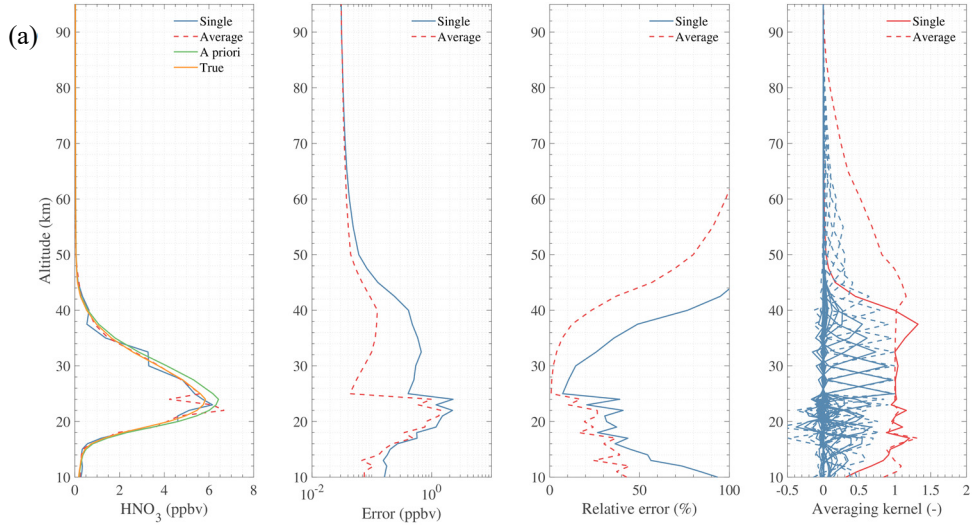

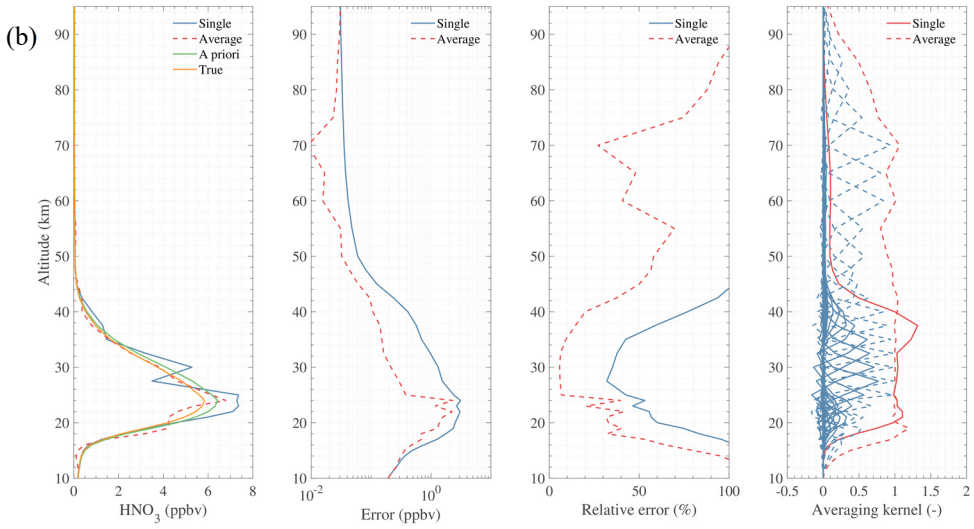

Figure 15. Simulation results of HNO_3 retrieval using 244 (a), and 656 GHz (b) lines.

Figure 16 shows the expected precision of HCl observation. HCl can be measured at 25–50 km with < 20% single scan relative error. The vertical resolution is 2.5–5 km through most of the useful range. By averaging the measurements, the precision will be < 5% at 25–65 km.

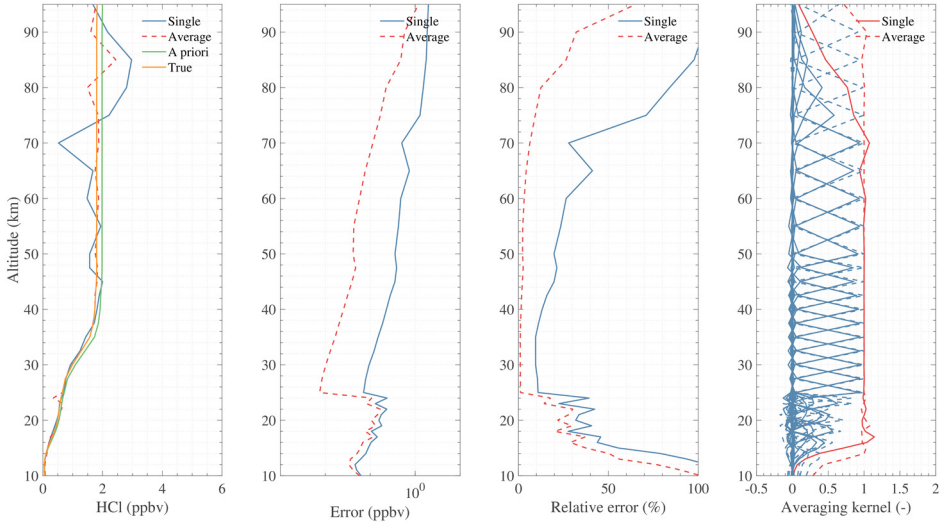

Figure 16. Simulation result of HCl retrieval using 624.9 GHz lines.

N_2O can be retrieved from the band at 190 GHz in the upper troposphere while the band at 643 GHz can provide more information in the stratosphere. Figure 17 shows that single scan precision of 190 GHz is < 40% at 10–35 km with the vertical resolution of 2.5–5 km. By averaging the measurements, the precision will be < 30% from 10 to 45 km. The 643 GHz can give the similar precision at 15–50 km.

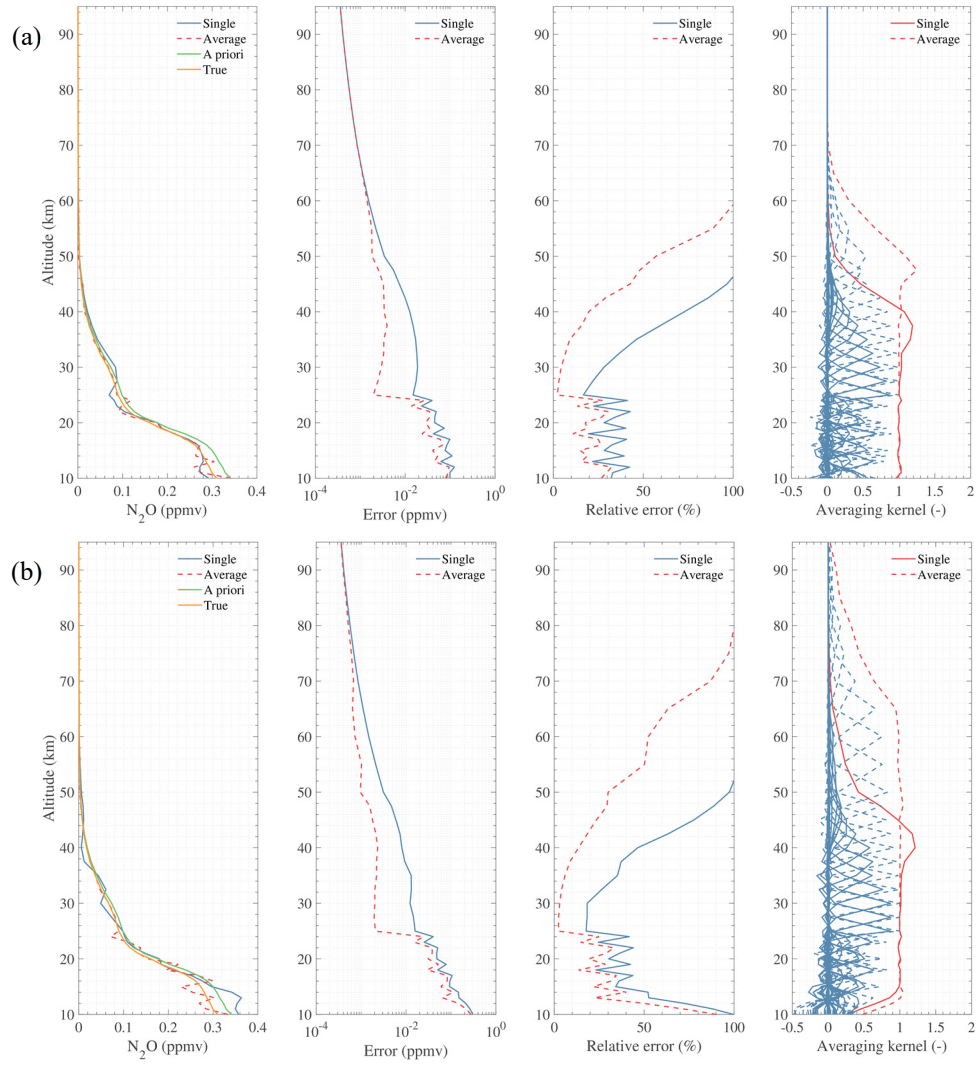

Figure 17. Simulation results of N_2O retrieval using 200.98 (a), and 652.834 GHz (b) lines.

ClO can be retrieved from radiances measured by 190 and 643 GHz bands (Fig. 18). However, the result shows that the best retrievals are performed from the band at 643 GHz but information can also be retrieved from the 190 GHz radiometer with less precision. Single scan measurement from 643 GHz radiometer can be used to obtain ClO with 30–50% precision from 30 to 45 km, and the vertical resolution is about 3–4 km throughout the useful range. By averaging the measurements, precision will be 5–30% from 25 to 60 km.

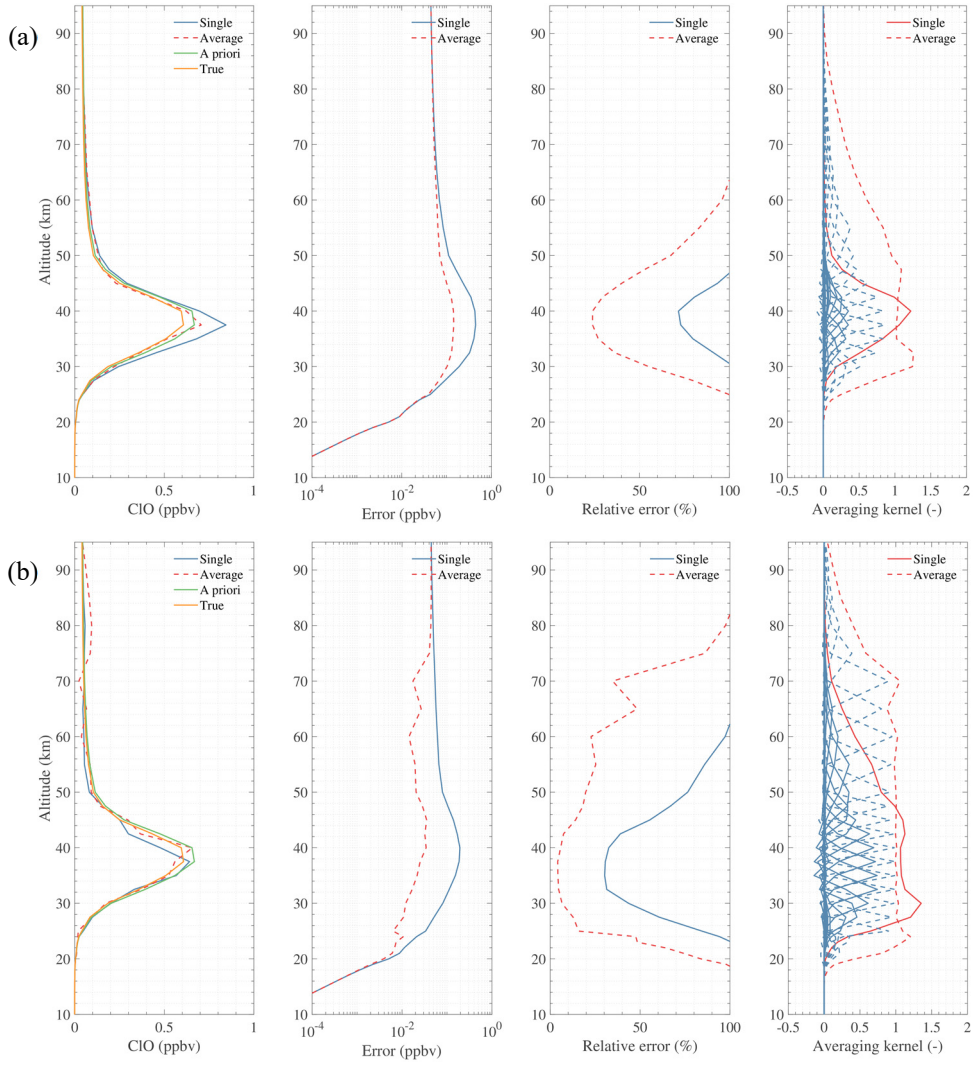

Figure 18. Simulation results of ClO retrieval using 203.4 (a) and 649.45 GHz (b) lines.

4.3.2 Medium precision products

Medium precision products including CO, HCN, CH_3Cl mean that their single scan retrieval precisions are not satisfying, but can be used to some degree. There is a choice for the user to select the single scan or averaged products.

CO can be measured using 230.538 and 661.07 GHz lines. Figure 19 shows that the 240 GHz radiometer can provide CO information with 40–90% single scan precision from 10 to 70 km. The vertical resolution is in the range 3.5–5.5 km from the upper troposphere to the lower mesosphere, degrading to 6–10 km in the upper mesosphere. By using averaged measurements, CO can be retrieved with < 40% relative error from 10 to 25 km, < 20% relative error at the range of 25–95 km. However, the retrieval of 643 GHz measurement shows poor precision.

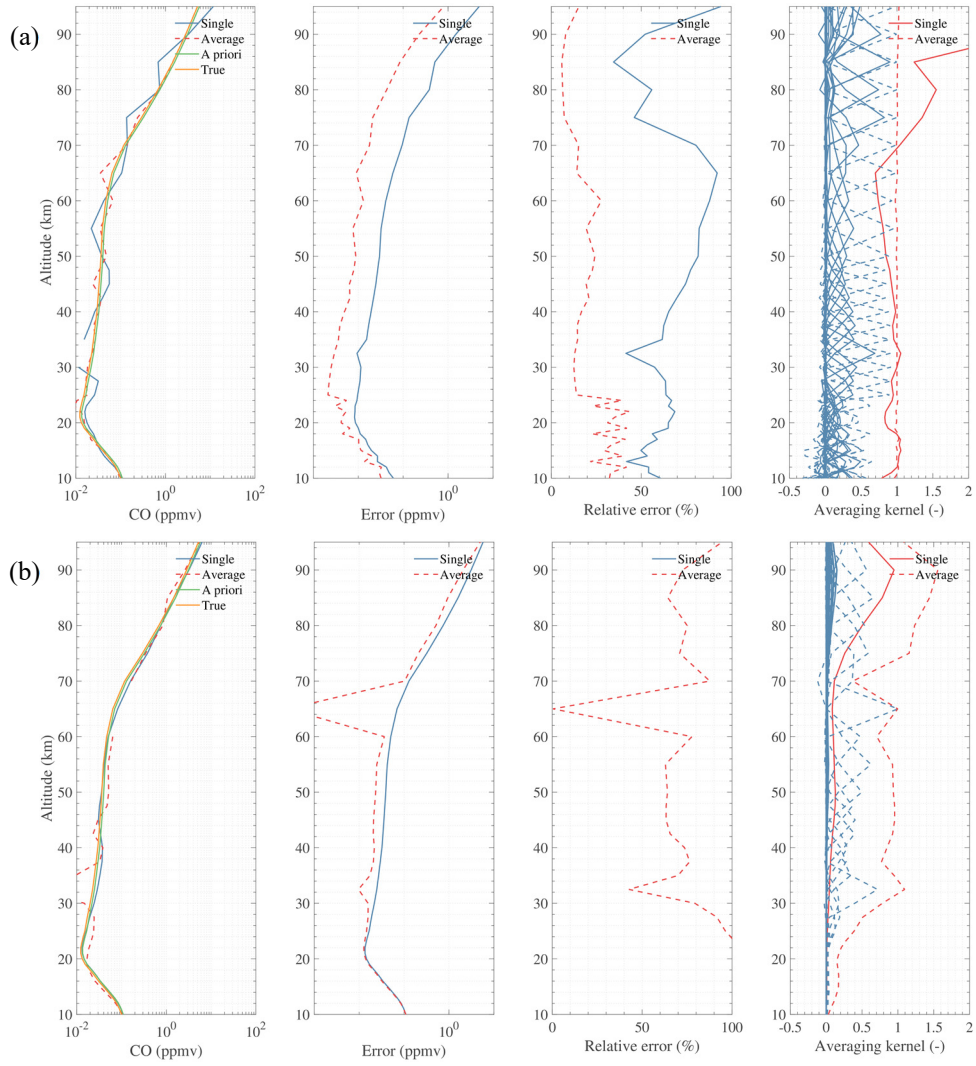

Figure 19. Simulation results of CO retrieval using 230.538 (a) and 661.07 GHz (b) lines.

HCN is measured by 190 GHz radiometer at 177.26 GHz line. The single scan precision is around 50% from 18 to 32 km and the vertical resolution is about 5 km at the height of 30 km, degrading to 8 km at about 40 km (Fig. 20). By averaging the measurements, the relative error will be < 50% at 15–60 km.

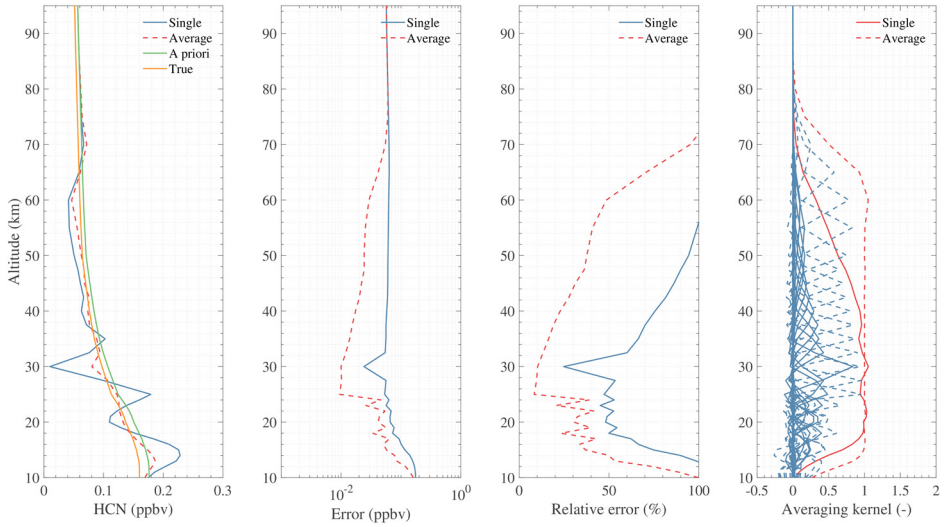

Figure 20. Simulation result of HCN retrieval using 177.26 GHz line.

CH_3Cl can be measured by the 643 GHz radiometer. As the result shows (Fig. 21), the 649.5 GHz band are suitable for CH_3Cl observation in the upper troposphere and lower stratosphere. It can be measured with 40–50% single scan precision from 15 to 23 km, with 20–50% averaged precision from 12 to 30 km. The vertical resolution is about 3 km over most of the useful range.

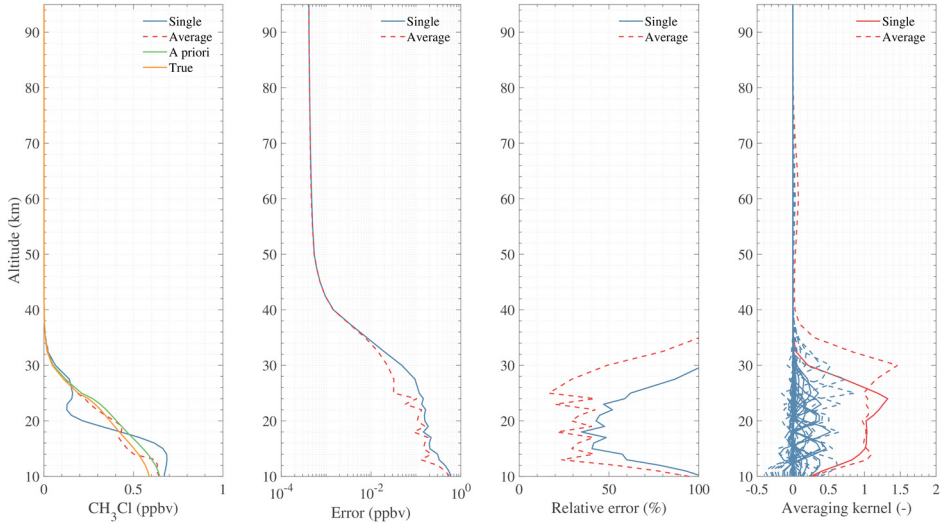

Figure 21. Simulation results of CH_3Cl retrieval using 649.5 GHz lines.

4.3.3 Low precision products

There are several weak lines in the spectral regions of TALIS such as HOCl, BrO, and HO_2. Significantly average must be done to these measurements in order to obtain reliable and satisfying precision.

The 635.87 GHz line is the most appropriate line for HOCl observation. However, the single scan retrieval has poor precision of 70–100% with the vertical resolution of about 6 km. Figure 22 reveals that HOCl can be retrieved from 22 to 52 km with averaged measurement precision of 15–50%.

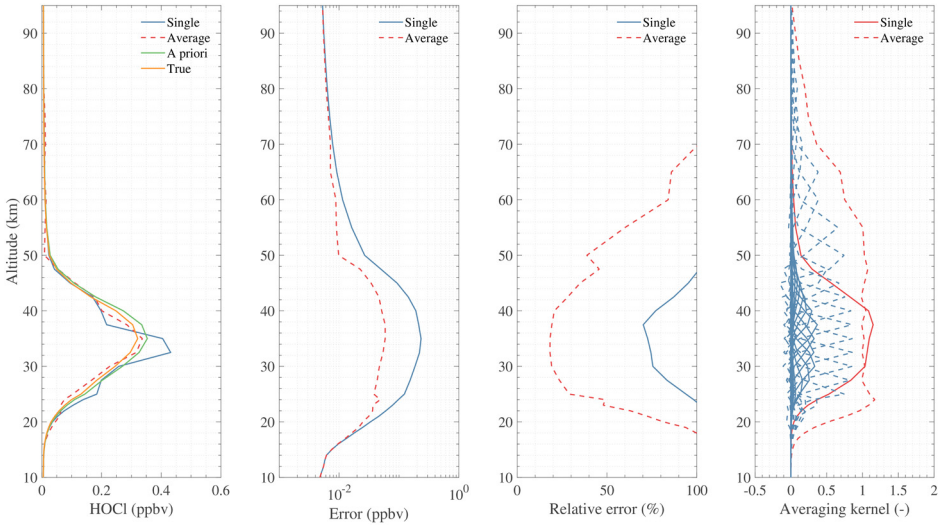

Figure 22. Simulation result of HOCl retrieval using 635.87 GHz line.

BrO can be measured by using 624.768 GHz spectral line. Figure 23 shows the simulation result of BrO retrieval. As the averaging kernel reveals, there is almost no useful information in single scan measurement because of the quite poor signal-to-noise ratio. Therefore, averaging is needed to obtain reliable and scientific results. The error is 50–80% from 23 to 56 km with the vertical resolution of about 4 km.

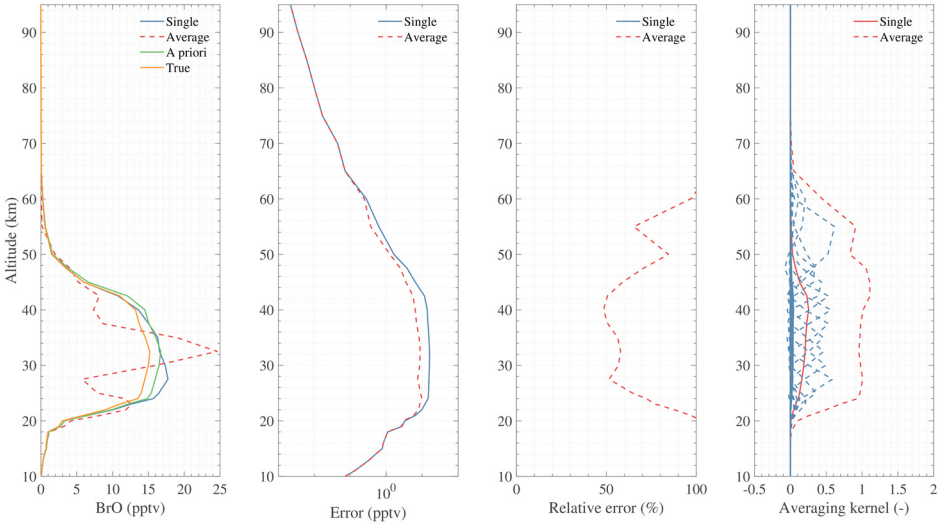

Figure 23. Simulation results of BrO retrieval using 624.768 GHz line.

HO_2 can be measured by the 643 GHz radiometer with 10–50% precision at the vertical range of 35–85 km by using averaged data (Fig. 24). The precision of single scan retrieval is not desirable because of the weak signal. The vertical resolution is about 6 km.

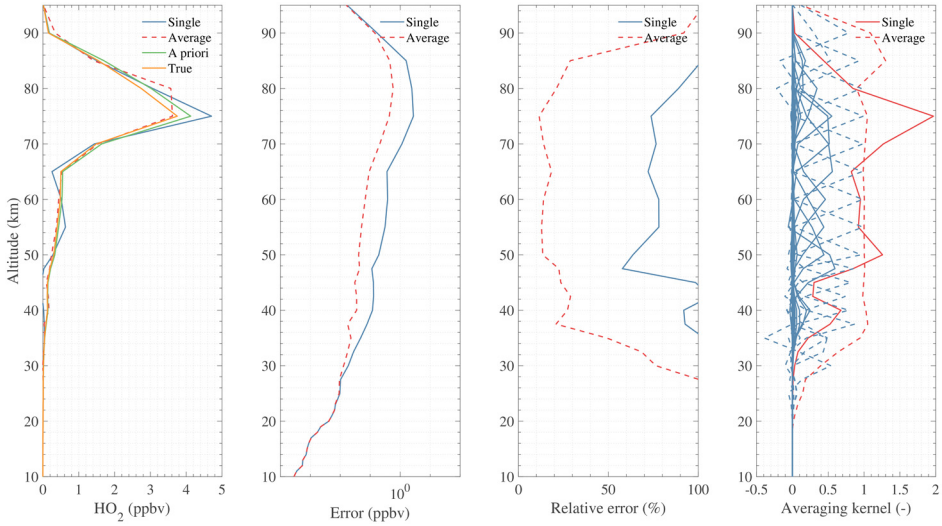

Figure 24. Simulation results of HO_2 retrieval using 649.701 GHz line.

4.3.4 Promising products

The unique products are the target species which are not covered by EOS MLS but covered by TALIS. There are four gases: NO, NO_2, H_2CO, and SO_2 (normal VMR). However, their signals all have weak intensity and must be averaged to improve the retrieval precision.

NO (daytime) can be retrieved from averaged data with 10–40% precision at 30–95 km (Fig. 25) while it vanishes in the nighttime. The vertical resolution is about 6 km. While its single scan measurement has no information in the area where NO largely exists.

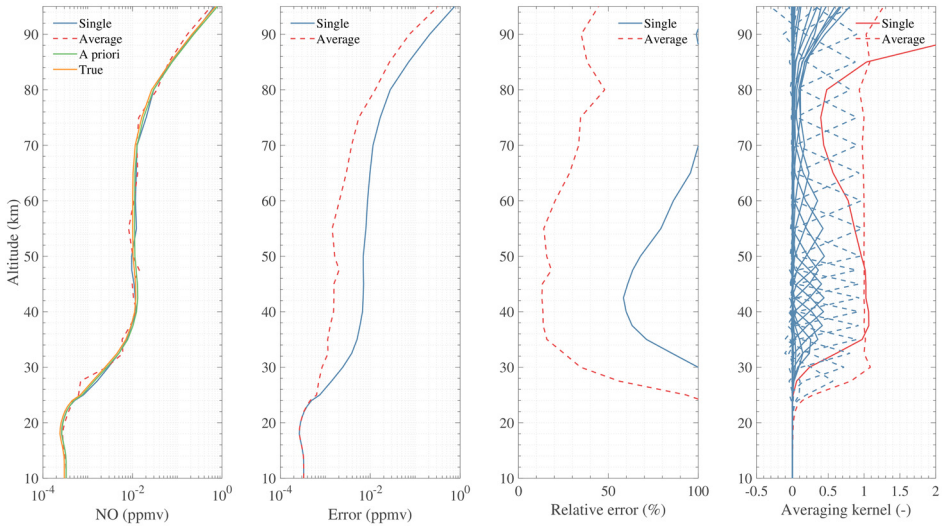

Figure 25. Simulation result of NO retrieval using 651.75 GHz line.

NO_2 (nighttime) has a weak line in the spectrum of 240 GHz band and it vanishes in the daytime. Figure 26 shows that only averaged measurement can provide some information at 25–40 km with the precision of about 50% in the nighttime. The vertical resolution is about 5 km.

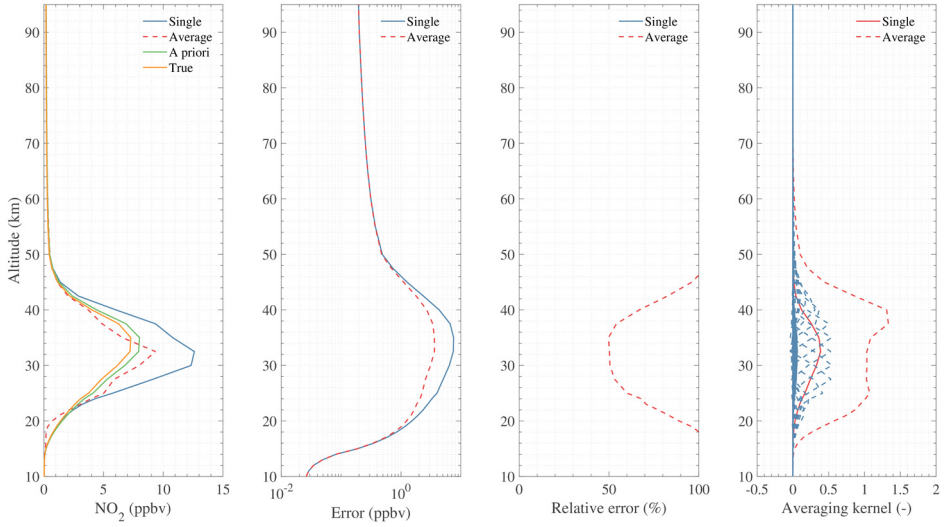

Figure 26. Simulation result of NO_2 retrieval using 232.7 GHz lines.

Although H_2CO has a line at 656.45 GHz, its emission radiance is too weak. Almost no useful information can be obtained (Fig. 27). However, this line has the potential to measure H_2CO. More average or other effective methods should be applied to get acceptable precision.

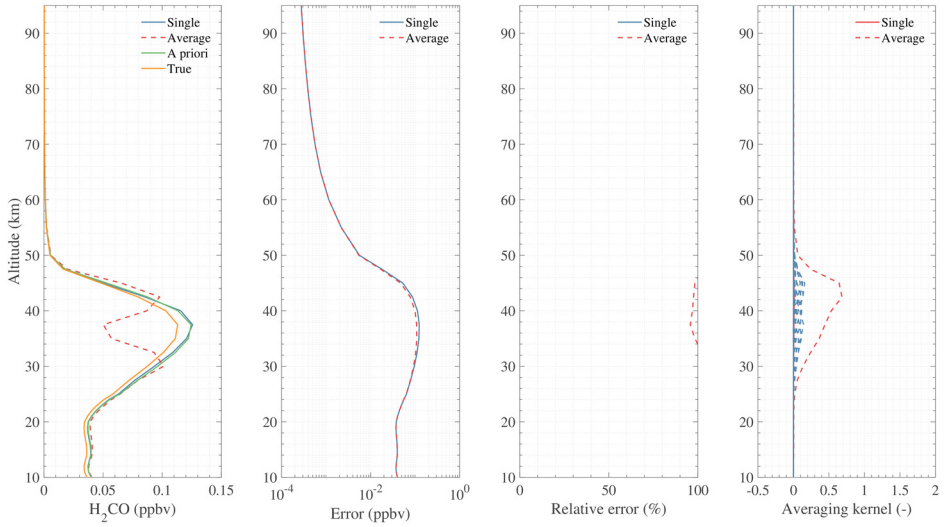

Figure 27. Simulation result of H_2CO retrieval using 656.45 GHz line.

MLS standard SO_2 product is taken from the 240 GHz retrieval, but only effective when its concentration significantly enhanced. TALIS has both 240 and 643 GHz radiometer which covering the lines of SO_2. The 240 GHz radiometer can be used to measure SO_2 like the way of MLS. The 643 GHz radiometer can give the concentration of nominal background. The averaged result shows that SO_2 can be retrieved at 40–75 km with the relative error about 20–60% (Fig. 28). The vertical resolution is about 6 km.

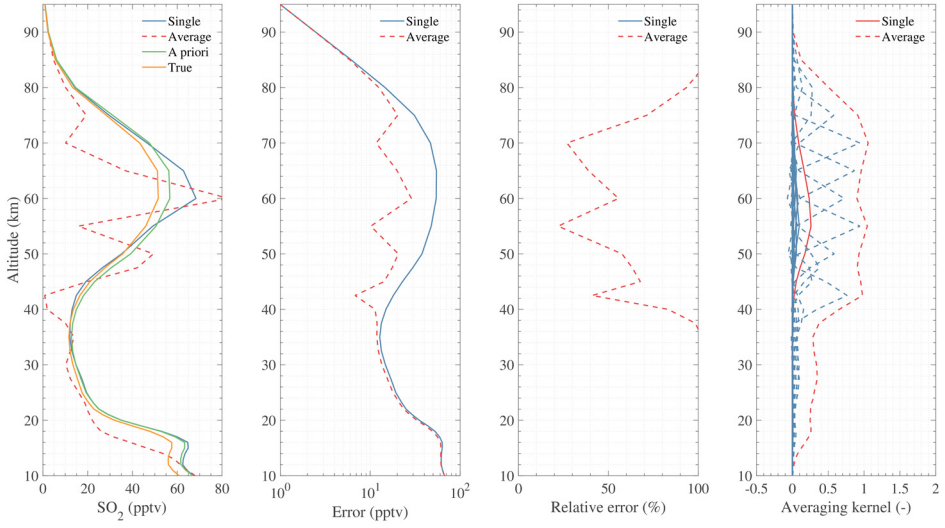

Figure 28. Simulation result of SO_2 retrieval using 659 GHz lines.

5 Conclusions

Simulation analysis for temperature and chemical species retrieval have been performed to assess the measurement performance of TALIS and to support the mission. This study mainly focuses on a large number of important chemical species in middle and upper atmosphere which can be observed by limb sounder. The results are summarized in Table 3.

The results of seven high sensitivity products are reliable. 118, 240, and 643 GHz observations of O_2 are used to estimate temperature profile which is quite important in meteorology. The 118 GHz radiometer can obtain temperature with a precision < 2 K at 15–80 km and the 240 and 643 GHz radiometers can provide information in the upper troposphere. The 190 GHz radiometer can be used to measure H_2O with a precision < 10% in a wide vertical range and give information of upper tropospheric humidity. O_3 can be measured by three radiometers, and the 240 GHz radiometer has the best precision. The precision is < 5% from 25 to 60 km by single scan measurement. HNO_3 can be derived from 240 GHz retrieval with a precision < 40%. The result of HCl single scan retrieval is < 40% over most of the useful range. The 190 GHz radiometer can give a good estimate to N_2O profile with a precision about 20–40%, while 643 GHz measurement can provide more information at higher altitudes. Single scan precision of ClO measured by 643 GHz radiometer is about 30% in the area where ClO mainly exists. CH_3Cl can be measured in the upper troposphere and low stratosphere with a precision about 50%. The profile of CO retrieved from 240 GHz measurement is better than that from 643 GHz measurement. The best sensitivity is found between 70~90 km where the VMR of CO is large, and the precision is better than 50%. HCN have 50% single scan precision at 18–32 km which may need to be averaged. Other measurements such as HO_2, HOCl, NO, NO_2, BrO, SO_2, and H_2CO must be significantly averaged before scientific use because of the weak signals. As the results show that the precision of some products become much poorer suddenly at a height of 25 km, it seems that the retrieval grid resolution does not match the achievable resolution.

Apart from these products, some potential products will be discussed in the future works. Line-of-sight wind is important information which could be measured by TALIS. Cloud IceWater Content (IWC) is also an essential product provided by passive microwave radiometer. Future studies will also investigate the Zeeman effect as it polarizes and changes the shape of the O_2 lines.

TALIS has strong potential to monitor chemical composition in the whole Earth's atmosphere which is important for numerical weather prediction models and to characterize the long-time change of climate. Measurement data can be used for atmospheric chemistry and dynamics study which is quite important for the geoscience. A better understanding of the key chemical and dynamical processes in the middle and upper atmosphere will help us solve the climate problem more efficient.

This paper is the preliminary analysis of the instrument. More studies such as structure optimization, calibration research, and error analysis will be performed to support the mission.

Table 3. Simulation results of TALIS retrieval precision

Product	Radiometer	Single precision	Average precision
Temperature	118 GHz, 240 GHz	< 2K (10–75 km)	< 1K (10–85 km)

H_2O	190 GHz	< 10% (25–75 km)	~ 1% (25–80 km)
O_3	240 GHz	< 5% (25–55 km)	~ 1% (25–70 km)
HCl	643 GHz	10–50% (15–70 km)	< 10% (25–75 km)
N_2O	190 GHz, 643 GHz	20–40% (10–40 km)	< 40% (10–50 km)
HNO_3	240 GHz	10–50% (15–35 km)	< 50% (10–45 km)
ClO	643 GHz	30–50% (30–45 km)	< 30% (25–60 km)
CO	240 GHz	40–90% (10–70 km)	< 40% (10–95 km)
HCN	190 GHz	20–50% (18–32 km)	10–50% (15–60 km)
CH_3Cl	643 GHz	40–50% (15–23 km)	20–50% (12–30 km)
HOCl	643 GHz	70–90% (27–43 km)	15–50% (22–52 km)
BrO	643 GHz	/	50–80% (23–56 km)
HO_2	643 GHz	60–80% (47–67 km)	10–50% (35–85 km)
NO	643 GHz	60–80% (33–55 km)	10–40% (30–95 km)
NO_2	240 GHz	/	50–60% (25–40 km)
H_2CO	643 GHz	/	/
SO_2	643 GHz	/	20–60% (40–75 km)

Code and data availability. ARTS can be downloaded at http://www.radiativetransfer.org/getarts/. Qpack is included in the Atmlab which can be downloaded from http://www.radiativetransfer.org/tools/. Profiles and spectroscopy data of Perrin and HITRAN are included in ARTS XML Data. JPL molecular spectroscopy catalogue is available at https://spec.jpl.nasa.gov/. MLS version 4.2 data can be obtained at https://doi.org/10.5067/Aura/MLS/DATA3020.

Author contribution. Zhenzhan Wang designed the mission concept. Wenyu Wang performed the simulate and wrote the manuscript. Wenyu Wang and Yongqiang Duan analysed the results. Zhenzhan Wang edited the article.

Competing interests. The authors declare that they have no conflict of interest.

Acknowledgements. The authors would like to thank the ARTS and Qpack development teams for assistance configuring and running the model. The authors thank the JPL for providing spectroscopy data and MLS data. They would also like to thank the reviewers and the editors for their valuable and helpful suggestions.

References

Baron, P., Ricaud, P., de la Nöe, J., Eriksson, P., Merino, F., Ridal, M., and Murtagh, D. P.: Studies for the Odin Sub-Millimetre Radiometer. II. Retrieval methodology, Can. J. Phys., 80, 341–356, https://doi.org/10.1139/P01-150, 2002.

Baron, P., Urban, J., Sagawa, H., Möller, J., Murtagh, D. P., Mendrok, J., Dupuy, E., Sato, T. O., Ochiai, S., Suzuki, K., Manabe, T., Nishibori, T., Kikuchi, K., Sato, R., Takayanagi, M., Murayama, Y., Shiotani, M., and Kasai, Y.: The Level 2 research product algorithms for the Superconducting Submillimeter-Wave Limb-Emission Sounder (SMILES), Atmos. Meas. Tech., 4, 2105-2124, https://doi.org/10.5194/amt-4-2105-2011, 2011.

Baron, P., Murtagh, D. P., Urban, J., Sagawa, H., Ochiai, S., Kasai, Y., Kikuchi, K., Khosrawi, F., Körnich, H., Mizobuchi, S., Sagi, K., and Yasui, M.: Observation of horizontal winds in the middle-atmosphere between 30°S and 55°N during the northern winter 2009–2010, Atmos. Chem. Phys., 13, 6049–6064, https://doi.org/10.5194/acp-13-6049-2013, 2013.

Baron, P., Murtagh, D., Eriksson, P., Mendrok, J., Ochiai, S., Pérot, K., Sagawa, H., and Suzuki, M.: Simulation study for the Stratospheric Inferred Winds (SIW) sub-millimeter limb sounder, Atmos. Meas. Tech., 11, 4545-4566, https://doi.org/10.5194/amt-11-4545-2018, 2018.

Bremer, J. C.: Improvement of Scanning Radiometer Performance by Digital Reference Averaging, IEEE. T. INSTRUM. MEAS., 28, 46–54, https://10.1109/TIM.1979.4314759, 1979.

Eriksson, P., Jiménez, C., and Buehler, S. A.: Qpack, a general tool for instrument simulation and retrieval work, J. Quant. Spectrosc. Ra., 91, 47–64, https://doi.org/10.1016/j.jqsrt.2004.05.050, 2005.

Eriksson, P., Ekström, M., Melsheimer, C., and Buehler, S. A.: Efficient forward modelling by matrix representation of sensor responses, Int. J. Remote Sens., 27, 1793–1808, https://doi.org/10.1080/01431160500447254, 2006.

Eriksson, P., Ekström, M., Rydberg, B., and Murtagh, D. P.: First Odin sub-mm retrievals in the tropical upper troposphere: ice cloud properties, Atmos. Chem. Phys., 7, 471-483, https://doi.org/10.5194/acp-7-471-2007, 2007.

Eriksson, P., Buehler, S. A., Davis, C. P., Emde, C., and Lemke, O.: ARTS, the atmospheric radiative transfer simulator, Version 2, J. Quant. Spectrosc. Ra., 112, 1551–1558, https://doi.org/10.1016/j.jqsrt.2011.03.001, 2011.

Johnson, D. G., Traub, W. A., Chance, K. V., Jucks, K. W., and Stachnik, R. A.: Estimating the abundance of ClO from simultaneous remote sensing measurements of HO_2, OH, and HOCl, Geophys. Res. Lett., 22, 1869–1871, https://doi.org/10.1029/95GL01249, 1995.

Kasai, Y., Sagawa, H., Kreyling, D., Dupuy, E., Baron, P., Mendrok, J., Suzuki, K., Sato, T. O., Nishibori, T., Mizobuchi, S., Kikuchi, K., Manabe, T., Ozeki, H., Sugita, T., Fujiwara, M., Irimajiri, Y., Walker, K. A., Bernath, P. F., Boone, C., Stiller, G., von Clarmann, T., Orphal, J., Urban, J., Murtagh, D., Llewellyn, E. J., Degenstein, D., Bourassa, A. E., Lloyd, N. D., Froidevaux, L., Birk, M., Wagner, G., Schreier, F., Xu, J., Vogt, P., Trautmann, T., and Yasui, M.: Validation of stratospheric and mesospheric ozone observed by SMILES from International Space Station, Atmos. Meas. Tech., 6, 2311–2338, https://doi.org/10.5194/amt-6-2311-2013, 2013.

Kikuchi, K., Nishibori, T., Ochiai, S., Ozeki, H., Irimajiri, Y., Kasai, Y., Koike, M., Manabe, T., Mizukoshi, K., Murayama, Y., Nagahama, T., Sano, T., Sato, R., Seta, M., Takahashi, C., Takayanagi, M., Masuko, H., Inatani, J., Suzuki, M., and Shiotani, M.: Overview and early results of the Superconducting Submillimeter-Wave Limb-Emission Sounder (SMILES), J. Geophys. Res.-Atmos., 115, D23306, https://doi.org/10.1029/2010JD014379, 2010.

Lambert, A., Read, W. G., Livesey, N. J., Santee, M. L., Manney, G. L., Froidevaux, L., Wu, D. L., Schwartz, M. J., Pumphrey, H. C., Jimenez, C., Nedoluha, G. E., Cofield, R. E., Cuddy, D. T., Daffer, W. H., Drouin, B. J., Fuller, R. A., Jarnot, R. F., Knosp, B. W., Pickett, H. M., Perun, V. S., Snyder, W. V., Stek, P. C., Thurstans, R. P., Wagner, P. A., Waters, J. W., Jucks, K. W., Toon, G. C., Stachnik, R. A., Bernath, P. F., Boone, C. D., Walker, K. A., Urban, J., Murtagh, D., Elkins, J. W., and Atlas, E.: Validation of the Aura Microwave Limb Sounder middle atmosphere water vapor and nitrous oxide measurements, J. Geophys. Res.-Atmos., 112, D24S36, https://doi.org/10.1029/2007JD008724, 2007.

Livesey, N. J. and Snyder, W. V.: EOS MLS Retrieval Processes Algorithm Theoretical Basis., Tech. Rep. JPL D-16159 / CL #04-2043, Jet Propulsion Laboratory, California Institute of Technology, Pasadena, California, 91109-8099, available at: https://mls.jpl.nasa.gov/data/eos_algorithm_atbd.pdf (last access: 26 March 2019), version 2.0, 2004.

Livesey, N. J., Filipiak, M. J., Froidevaux, L., Read, W. G., Lambet, A., Santee, M. L., Jiang, J. H., Pumphrey, H. C., Waters, J. W., Cofield, R. E., Cuddy, D. T., Daffer, W. H., Drouin, B. J., Fuller, R. A., Jarnot, R. F., Jiang, Y. B., Knosp, B. W., Li, Q. B., Perun, V. S., Schwartz, M. J., Snyder, W. V., Stek, P. C., Thurstans, R. P., Wagner, P. A., Avery, M., Browell, E. V., Cammas, J. P., Christensen, L. E., Diskin, G. S., Gao, R. S., Jost, H. J., Loewenstein, M., Lopez, J. D., Nedelec, P., Osterman, G. B., Sachse, G. W., and Webster, C. R.: Validation of Aura Microwave Limb Sounder O_3 and CO observations in the upper troposphere and lower stratosphere, J. Geophys. Res.-Atmos., 113, D15S02, https://doi.org/10.1029/2007JD008805, 2008.

Livesey, N. J., Logan, J. A., Santee, M. L., Waters, J. W., Doherty, R. M., Read, W. G., Froidevaux, L., and Jiang, J. H.: Interrelated variations of O_3, CO and deep convection in the tropical/subtropical upper troposphere observed by the Aura Microwave Limb Sounder (MLS) during 2004–2011, Atmos. Chem. Phys., 13, 579-598, https://doi.org/10.5194/acp-13-579-2013, 2013.

Livesey, N. J., Read, W. G., Wagner, P. A., Froidevaux, L., Lambert, A., Manney, G. L., Millán, L. F., Pumphrey, H. C., Santee, M. L., Schwartz, M. J., Wang, S. H., Fuller, R. A., Jarnot, R. F., Knosp, B. W., Martinez, E., Lay, R. R.: Earth Observing System (EOS) Aura Microwave Limb Sounder (MLS) Version 4.2x Level 2 data quality and description document., Tech. Rep. JPL D-33509 Rev. D, Jet Propulsion Laboratory, California Institute of Technology, Pasadena, California, 91109-8099, available at: https://mls.jpl.nasa.gov/data/v4-2_data_quality_document.pdf (last access: 26 March 2019), Version 4.2x–3.1, 2018.

Marks, C. J. and Rodgers, C. D.: A retrieval method for atmospheric composition from limb emission measurements, J. Geophys. Res.-Atmos., 98, 14939–14953, https://doi.org/10.1029/93JD01195, 1993.

Mätzler, C.: Thermal Microwave Radiation: Applications for Remote Sensing, vol. 52, Iet, 2006.

Millán, L., Livesey, N., Read, W., Froidevaux, L., Kinnison, D., Harwood, R., MacKenzie, I. A., and Chipperfield, M. P.: New Aura Microwave Limb Sounder observations of BrO and implications for Br_y, Atmos. Meas. Tech., 5, 1741-1751, https://doi.org/10.5194/amt-5-1741-2012, 2012.

Millán, L., Wang, S., Livesey, N., Kinnison, D., Sagawa, H., and Kasai, Y.: Stratospheric and mesospheric HO_2 observations from the Aura Microwave Limb Sounder, Atmos. Chem. Phys., 15, 2889-2902, https://doi.org/10.5194/acp-15-2889-2015, 2015.

Murtagh, D., Frisk, U., Merino, F., Ridal, M., Jonsson, A., Stegman, J., Witt, G., Eriksson, P., Jimenez, C., Mégie, G., de la Nöe, J., Ricaud, P., Baron, P., Pardo, J., Hauchcorne, A., Llewellyn, E., Degenstein, D., Gattinger, R., Lloyd, N., Evans, W., McDade, I., Haley, C., Sioris, C., von Savigny, C., Solheim, B., McConnell, J., Strong, K., Richardson, E., Leppelmeier, G., Kyrola, E., Auvinen, H., and Oikarinen, L.: An overview of the Odin atmospheric mission, Can. J. Phys., 80, 309–319, https://doi.org/10.1139/P01-157, 2002.

Ochiai, S., Baron, P., Nishibori, T., Irimajiri, Y., Uzawa, Y., Manabe, T., Maezawa, H., Mizuno, A., Nagahama, T., Sagawa, H., Suzuki, M., and Shiotani, M.: SMILES-2 Mission for Temperature, Wind, and Composition in the Whole Atmosphere, SOLA, 13A, 13–18, https://doi.org/10.2151/sola.13A-003, 2017.

Perrin, A., Puzzarini. C., Colmont, J.-M., Verdes, C., Wlodarczak, G., Cazzoli, G., Buehler, S., Flaud, J.-M., and Demaison, J.: Molecular Line Parameters for the "MASTER" (Millimeter Wave Acquisitions for Stratosphere/Troposphere Exchange Research) Database, J. Atmos. Chem, 51, 161-205, https://doi.org/10.1007/s10874-005-7185-9, 2005.

Pickett, H. M., Poynter, R. L., Cohen, E. A., Delitsky, M. L., Pearson, J. C., and Muller, H. S. P.: Submillimeter, millimeter, and microwave spectral line catalog, J. Quant. Spectrosc. Ra., 60, 883–890, https://doi.org/10.1016/S0022-4073(98)00091-0, 1998.

Pumphrey, H. C., Santee, M. L., Livesey, N. J., Schwartz, M. J., and Read, W. G.: Microwave Limb Sounder observations of biomass-burning products from the Australian bush fires of February 2009, Atmos. Chem. Phys., 11, 6285-6296, https://doi.org/10.5194/acp-11-6285-2011, 2011.

Pumphrey, H. C., Read, W. G., Livesey, N. J., and Yang, K.: Observations of volcanic SO_2 from MLS on Aura, Atmos. Meas. Tech., 8, 195-209, https://doi.org/10.5194/amt-8-195-2015, 2015.

Rodgers, C. D.: Inverse Methods for Atmospheric Sounding: Theory and Practice, World Scientific, Singapore, 2000.

Rothman, L. S., Gordon, I. E., Babikov, Y., Barbe, A., ChrisBenner, D., Bernath, P. F., Birk, M., Bizzocchi, L., Boudon,V., Brown, L. R., Campargue, A., Chance, K., Cohen, E. A., Coudert, L. H., Devi, V. M., Drouin, B. J., Fayt, A., Flaud,J.-M., Gamache, R. R., Harrison, J. J., Hartmann, J. -M., Hill, C., Hodges, J. T., Jacquemart, D., Jolly, A., Lamouroux, J., Le Roy, R. J., Li, G., Long, D. A., Lyulin, O. M., Mackie, C. J., Massie, S. T., Mikhailenko, S., Müller, H. S. P., Nau-menko, O. V., Nikitin, A. V., Orphal, J., Perevalov, V., Per-rin, A., Polovtseva, E. R., Richard, C., Smith, M. A. H., Starikova, E., Sung, K., Tashkun, S., Tennyson, J., Toon, G. C., Tyuterev, V. G., and Wagner, G.: The HITRAN2012 molecular spectroscopic database, J. Quant. Spectrosc. Ra., 130, 4–50, https://doi.org/10.1016/j.jqsrt.2013.07.002, 2013.

Santee, M. L., Lambert, A., Read, W. G., Livesey, N. J., Manney, G. L., Cofield, R. E., Cuddy, D. T., Daffer, W. H., Drouin, B. J., Froidevaux, L., Fuller, R. A., Jarnot, R. F., Knosp, B. W., Perun, V. S., Snyder, W. V., Stek, P. C., Thurstans, R. P., Wagner, P. A., Waters, J. W., Connor, B., Urban, J., Murtagh, D., Ricaud, P., Barrett, B., Kleinböhl, A., Kuttippurath, J., Küllmann, H., von Hobe, M., Toon, G. C., and Stachnik, R. A.: Validation of the Aura Microwave Limb Sounder ClO measurements, J. Geophys. Res.-Atmos., 113, D15S22, https://doi.org/10.1029/2007JD008762, 2008.

Sato, T. O., Sagawa, H., Kreyling, D., Manabe, T., Ochiai, S., Kikuchi, K., Baron, P., Mendrok, J., Urban, J., Murtagh, D., Yasui, M., and Kasai, Y.: Strato-mesospheric ClO observations by SMILES: error analysis and diurnal variation, Atmos. Meas. Tech., 5, 2809-2825, https://doi.org/10.5194/amt-5-2809-2012, 2012.

Suzuki, M., Manago, N., Ozeki, H., Ochiai, S., and Baron, P.: Sensitivity study of smiles-2 for chemical species, in: Sensors, Systems, and Next-Generation Satellites XIX, Toulouse, France, 16 October 2015, 15, 2015.

Swadley, S. D., Poe, G. A., Bell, W., Hong, Y., Kunkee, D. B., McDermid, I. S., and Leblanc, T.: Analysis and Characterization of the SSMIS Upper Atmosphere Sounding Channel Measurements, IEEE T. Geosci. Remote, 46, 962–983, https://doi.org/10.1109/TGRS.2008.916980, 2008.

Takahashi, C., Ochiai, S., and Suzuki, M.: Operational retrieval algorithms for JEM/SMILES level 2 data processing system, J. Quant. Spectrosc. Ra., 111, 160–173, https://doi.org/10.1016/j.jqsrt.2009.06.005, 2010.

Takahashi, C., Suzuki, M., Mitsuda, C., Ochiai, S., Manago, N., Hayashi, H., Iwata, Y., Imai, K., Sano, T., Takayanagi, M., and Shiotani, M.: Capability for ozone high-precision retrieval on JEM/SMILES observation, Adv. Space Res., 48, 1076–1085, https://doi.org/10.1016/j.asr.2011.04.038, 2011.

Urban, J.: Optimal sub-millimeter bands for passive limb observations of stratospheric HBr, BrO, HOCl, and HO_2 from space, J. Quant. Spectrosc. Ra., 76, 145–178, https://doi.org/10.1016/s0022-4073(02)00051-1, 2003.

Urban, J., Baron, P., Lautié, N., Schneider, N., Dassas, K., Ricaud, P., and De la Nöe, J.: Moliere (v5): a versatile forward- and inversion model for the millimeter and sub-millimeter wavelength range, J. Quant. Spectrosc. Ra., 83, 529–554, https://doi.org/10.1016/S0022-4073(03)00104-3, 2004.

Urban, J., Lautié, N., Le Flochmoën, E., Jiménez, C., Eriksson, P., de la Nöe, J., Dupuy, E., Ekström, M., El Amraoui, L., Frisk, U., Murtagh, D., Olberg, M., and Ricaud, P.: Odin/SMR limb observations of stratospheric trace gases: Level 2 processing of ClO, N_2O, HNO_3, and O_3, J. Geophys. Res.-Atmos., 110, D14307, https://doi.org/10.1029/2004JD005741, 2005.

Waters, J. W., Froidevaux, L., Read, W. G., Manney, G. L., Elson, L. S., Flower, D. A., Jarnot, R. F., and Harwood, R. S.: Stratospheric ClO and ozone from the Microwave Limb Sounder on the Upper Atmosphere Research Satellite, Nature, 362, 597–602, https://doi.org/10.1038/362597a0, 1993.

Waters, J.W., Froidevaux, L., Jarnot, R.F., Read, W.G., Pickett, H.M., Harwood, R.S., Cofield, R.E., Filipiak, M. J., Flower, D. A., Livesey, N. J., Manney, G. L., Pumphrey, H. C., Santee, M. L., Siegel, P. H., and Wu, D. L.: An Overview of the EOS MLS Experiment., Tech. Rep. JPL D-15745 / CL# 04-2323, Jet Propulsion Laboratory, California Institute of

Technology, Pasadena, California, 91109-8099, available at: https://mls.jpl.nasa.gov/data/eos_overview_atbd.pdf (last access: 26 March 2019), Version 2.0, 2004.

Waters, J. W., Froidevaux, L., Harwood, R. S., Jarnot, R. F., Pickett, H. M., Read, W. G., Siegel, P. H., Cofield, R. E., Filipiak, M. J., Flower, D. A., Holden, J. R., Lau, G. K., Livesey, N. J., Manney, G. L., Pumphrey, H. C., Santee, M. L., Wu, D. L., Cuddy, D. T., Lay, R. R., Loo, M. S., Perun, V. S., Schwartz, M. J., Stek, P. C., Thurstans, R. P., Boyles, M. A., Chandra, K. M., Chavez, M. C., Chen, G.-S., Chudasama, B. V., Dodge, R., Fuller, R. A., Girard, M. A., Jiang, J. H., Jiang, Y., Knosp, B. W., LaBelle, R. C., Lam, J. C., Lee, K. A., Miller, D., Oswald, J. E., Patel, N. C., Pukala, D. M., Quintero, O., Scaff, D. M., Snyder, W. V., Tope, M. C., Wagner, P. A., and Walch, M. J.: The Earth Observing System Microwave Limb Sounder (EOS MLS) on the Aura Satellite, IEEE T. Geosci. Remote, 44, 1075–1092, https://doi.org/10.1109/TGRS.2006.873771, 2006.

Wu, D. L., Schwartz, M. J., Waters, J. W., Limpasuvan, V., Wu, Q., and Killeen, T. L.: Mesospheric doppler wind measurements from Aura Microwave Limb Sounder (MLS), Adv. Space Res., 42, 1246–1252, https://doi.org/10.1016/j.asr.2007.06.014, 2008.